IOPscience iopscience.iop.org

Home Search Collections Journals About Contact us My IOPscience

Semiconductor ultraviolet photodetectors based on ZnO and $Mg_xZn_{1-x}O$

This content has been downloaded from IOPscience. Please scroll down to see the full text.

2014 J. Phys. D: Appl. Phys. 47 283001

(http://iopscience.iop.org/0022-3727/47/28/283001)

View the table of contents for this issue, or go to the journal homepage for more

Download details:
This content was downloaded by: houyaonan
IP Address: 143.167.182.216
This content was downloaded on 25/06/2014 at 08:28

Please note that terms and conditions apply.

IOP Publishing

Journal of Physics D: Applied Physics

J. Phys. D: Appl. Phys. **47** (2014) 283001 (25pp)

doi:10.1088/0022-3727/47/28/283001

Topical Review

Semiconductor ultraviolet photodetectors based on ZnO and $Mg_xZn_{1-x}O$

Yaonan Hou, Zengxia Mei[1] and Xiaolong Du[1]

Key Laboratory for Renewable Energy, Beijing National Laboratory for Condensed Matter Physics, Institute of Physics, Chinese Academy of Sciences, Beijing 100190, People's Republic of China

E-mail: zxmei@iphy.ac.cn and xldu@iphy.ac.cn

Received 23 March 2014, revised 28 April 2014
Accepted for publication 2 May 2014
Published 24 June 2014

Abstract

It is indispensable to develop wide-band-gap based ultraviolet (UV) photodetectors (PDs), which are one of the basic building blocks of solid state UV optoelectronic devices. In the last two decades, we have witnessed the renaissance of ZnO as a wide-band-gap semiconductor and an enormous development of ZnO-based UV PDs as a result of its superb optical and electronic properties. Since the first demonstration, a great variety of UV PDs based on ZnO and its related materials have been proposed and demonstrated. These PDs, with diverse device geometries, exhibit either high performance or multiple functions, reflecting a state-of-the-art technology of UV optoelectronics. In this review, we study the latest progress of UV PDs made on ZnO and $Mg_xZn_{1-x}O$, which is a representative alloy of ZnO for band-gap engineering techniques. The discussion focuses on the device performance and the behind device physics according to the architecture of UV PDs.

Keywords: ZnO, $Mg_xZn_1 - xO$, UV photodetector, photoresponse

(Some figures may appear in colour only in the online journal)

1. Introduction

Ultraviolet (UV) detection has been attracting the attention of many researchers owing to its varied utility in modern civilian infrastructures, scientific research and military facilities, such as UV sterilization, flame detection, aerospace UV monitoring, UV analysis, inter-satellite covert communication and missile early warning [1–3]. Traditional UV photodetectors (PDs) are constructed in the form of pyroelectric devices, vacuum tubes, charge coupled devices (CCDs) and Si photodiodes. The common Si enhanced UV photodiodes still dominate the UV detection market, due to the well-established technology and low price. However, external filters are essentially needed to block the long-wavelength response to achieve UV detection, as the band gap of Si is only 1.1 eV. In the meantime, the photoresponsivity will be degraded somewhat due to the reflection of such high-pass filters, which is always compensated by using complicated external signal amplification circuits. Furthermore, the dark current of Si enhanced UV PDs often increases with temperature, attenuating the signal-to-noise ratio (S/N). Therefore, such UV detectors often suffer from low responsivity, low S/N ratio, low speed or bulky volume, which is incompatible with the demands of modern UV PDs.

Since the growth technology of the new generation wide-band-gap (WBG) semiconductors (for example, GaN and ZnO) has progressed substantially in the last two or three decades, more and more solid state UV PDs have been devised based on high-quality WBG semiconductors, which exhibit prospective applications for the future UV detection areas. Compared with traditional UV PDs, the WBG UV PDs not only possess the advantage of improved device performance but also can be miniaturized dramatically, and they do not need complicated external electrical power supplies or filters [4]. The commercialization of UV PDs based on GaN (and its alloys, $Al_xGa_{1-x}N$) is a milestone in the fast-developing WBG

[1] Authors to whom correspondence should be addressed.

 © 2014 IOP Publishing Ltd Printed in the UK

semiconductor based UV detection realm. Various studies on high-performance GaN based UV PDs can be found in several review articles [1, 5–7]. In contrast, ZnO with its alloys ($Mg_xZn_{1-x}O$) is recognized as an even more competitive candidate for fabrication of UV PDs due to several obvious advantages. For instance, as there is a lack of an appropriate substrate for homoepitaxial growth, the heteroexpitaxially grown $Al_xGa_{1-x}N$ has a dislocation density of 10^{7-9} cm^{-2}, which has an adverse effect on the performance of UV PDs [8]. Instead, $Mg_xZn_{1-x}O$ with a fairly low dislocation can be homoexpitaxially grown on ZnO substrate, which is evidenced by the recent observation of a fractional quantum Hall effect at the $Mg_xZn_{1-x}O$/ZnO interface [9]. Moreover, ZnO is more resistant to high-energy particle irradiation than GaN, which is extremely important for applications of UV PDs in outer space [10]. Simultaneously, substantial progress has been made on other WBG semiconductors including diamond and $\beta-Ga_2O_3$, symbolized by synthesis of their single-phase bulk wafers [11, 12]. Solid state UV PDs working in the solar-blind region under room light have also been successfully realized on these WBG semiconductors [13, 14].

1.1. Main parameters of WBG semiconductor UV PDs

Several main parameters are frequently used to characterize the performance of WBG semiconductor PDs, which are listed as the following.

(1) *Cutoff wavelength.* Cutoff wavelength is sometimes also called cutoff edge, and is closely related to the band-gap energy (E_g) of a semiconductor. For a WGB semiconductor PD, an effective photoresponse can be triggered only if the electron–hole pairs excited by the incident light enter the conduction and valence bands, respectively. Ideally, when the incident photon energy $hc/\lambda_{in} \geqslant E_g$, it can be absorbed and generate electron–hole pairs in a semiconductor. The cutoff edge is thus defined as the longest wavelength with the lowest photon energy absorbed by a specific semiconductor,

$$\lambda_c = hc/E_g = 1.24\,(\text{eV})\,/E_g \quad (\mu\text{m}) \tag{1.1}$$

where h, c, λ_{in} and λ_c are the Planck constant, light speed, incident light wavelength and cutoff wavelength. However, sometimes a photoresponse with photon energies lower than E_g can also be observed, known as the sub-band response, which is the response from carrier transitions relating to defect levels or band tails introduced by intrinsic defects or stacking faults formed during the synthesis procedure [15, 16].

(2) *Photoresponsivity* and *quantum efficiency.* Photoresponsivity is defined as the net photocurrent generated by unit illumination power at a specific wavelength,

$$R_p = I_{ph}/P_{opt} = (I_{tot} - I_{dark})\,/P_{opt} \tag{1.2}$$

where R_p, I_{ph}, I_{tot}, I_{dark} and P_{opt} are photoresponsivity, net photocurrent, total current under illumination, dark current and illumination power, respectively.

Quantum efficiency (η) is defined as the yield of carriers per incident photon. Together with equation (1.2), quantum efficiency can be expressed by

$$\eta = \left(I_{ph}/q\right)/\Phi = I_{ph}hc/q\lambda P_{opt} = R_p hc/q\lambda \tag{1.3}$$

where q, Φ and λ are electron charge, photon flux and wavelength of incident light, respectively. It is understandable that the quantum efficiency is a differential representation of the photoresponsivity.

(3) *S/N ratio.* It is important to suppress noise to obtain a good signal during PD operation. Normally, noise can be categorized as external and internal noise according to its origin. External noise is mainly the dark current generated by background radiation, while the internal noise comes from the thermal effect (Johnson noise), the statistical fluctuation (shot noise) and carrier recombination related to surface defects (flicker noise or $1/f$ noise [17]). Generally, the S/N ratio is intuitively expressed by the ratio of UV-to-dark responsivity of a WBG semiconductor PD, namely the rejection ratio.

(4) *Response speed.* The response speed represents the capability of a PD's transient response, which restricts the maximum bandwidth of the total circuits. Technically, the 10–90% response time is often used to characterize the response speed [4]. The 10–90% response time is defined as the time for the photocurrent to decrease from its maximum to 10% (or increase from dark to 90%).

(5) *Detectivity (D^*) and noise equivalent power (NEP).* Another two important parameters for a PD are detectivity and NEP, which characterizes the highest detection level of a PD from noises. In the case of white noise, the relationship between them can be expressed by

$$D^* = \sqrt{(A_{OOA} \times \Delta f)}/\text{NEP} \tag{1.4}$$

where A_{OOA} and Δf are the optical active area and electrical bandwidth of the PD, and NEP is defined as the optical output power in 1 Hz bandwidth, at which the S/N ratio is equal to one. Specifically, in the photovoltaic mode, the thermal-limited detectivity can be evaluated by [18]

$$D^* = R_p r_0 A_{OOA}/4kT \tag{1.5}$$

where R_p, r_0, k and T are the photoresponsivity, differential resistance at zero bias, Boltzmann constant and absolute temperature, respectively.

According to the architecture of the devices, UV PDs can be basically categorized as photoconductor, Schottky diode, p–n junction diode and hybrid functional detectors [19, 20]. Each kind of PD has one or more advantages against the others. This paper introduces the most recent development of UV PDs based on ZnO and its alloys ($Mg_xZn_{1-x}O$). We have arranged the context according to different device configurations in order to make our statements distinct.

1.2. General properties of ZnO and $Mg_xZn_{1-x}O$

ZnO is favoured for its numerous novel optoelectronic and chemical merits. With a WBG of 3.37 eV at room temperature and a large exciton binding energy of 60 meV [21], it is undoubtedly suitable for fabrication of optoelectronic devices in the UV range. Wet-etch availability and low synthesis temperature extensively simplify the device fabrication process. Its nature of radiation hardness and non-toxicity supports its application in a variety of environments. What is more, the low cost of raw material makes ZnO one of the most ascendant semiconductors for commercialization compared with its congeneric WBG semiconductors, such as III nitrides, diamond or SiC. Although the study of ZnO dates back to the 1930s and its UV response ability was first observed in the year 1956 [22, 23], it was impossible to fabricate high-performance UV PDs then as the intrinsic defect absorption could not be effectively suppressed [24]. Along with the development of growth techniques, a fast-response Schottky photodiode based on sputtered ZnO thin film was invented by the year 1986 [25]. Epitaxial technology has been applied for high-quality ZnO growth since the end of the 20th century, as in metal–organic chemical vapour deposition (MOCVD), molecular beam epitaxy (MBE), pulsed laser deposition (PLD) and so on [26–28]. From then on, ZnO-based UV PDs were vastly developed.

As is known, the UV light occupies a broad electromagnetic spectrum from 10 nm up to 400 nm. Thus WBG semiconductor based PDs with different cutoff wavelengths are always desired for practical applications, which undoubtedly require band-gap engineering techniques to achieve an appropriate band gap. In 1997, the ternary alloy $Mg_xZn_{1-x}O$ was proposed to be a good semiconductor for band-gap tailoring [29, 30]. It has a continuous tuneable band gap from 3.37 to 7.8 eV, covering most of the UV spectrum. Moreover, $Mg_xZn_{1-x}O$ inherits the unique optoelectronic properties from ZnO, which guarantees the device performance. However, due to the large difference of lattice structure between MgO (cubic with a lattice constant of 4.25 Å) and ZnO (wurzite with lattice constants of $a = 3.25$ Å, $c = 5.2$ Å [31]), synthesis of high-quality monocrystalline $Mg_xZn_{1-x}O$ is by no means an easy feat. Specifically, wurtzite $Mg_xZn_{1-x}O$ $(W - Mg_xZn_{1-x}O)$ with a high Mg content or cubic $Mg_xZn_{1-x}O$ $(C - Mg_xZn_{1-x}O)$ with a high Zn content (or low Mg content) tends to separate into wurtzite ZnO and cubic MgO mixtures during the growth, known as phase segregation. It has always been believed that the maximum Mg content x is 37% (4.28 eV) for $W - Mg_xZn_{1-x}O$ and the minimum 62% (5.4 eV) for $C - Mg_xZn_{1-x}O$, but $Mg_xZn_{1-x}O$ with a band gap of 4.28–5.4 eV is difficult to derive (figure 1) [32]. This discontinuity in band-gap engineering will have a fatal adverse effect on UV detection, let alone the fact that the missing part is one of the most important UV bands—the solar-blind region (220–280 nm). Fortunately, the limits have been broken down by improving the growth techniques, and now the band gap can be continuously tuned. With a quasi-homoepitaxial strategy, high-Mg-content $W - Mg_{0.55}Zn_{0.45}O$ was achieved in 2009, with the band gap of 4.55 eV in the solar-blind region [33, 34]. At the same time, $C - Mg_xZn_{1-x}O$ with x down to 30% was realized by the MBE growth method [35]. Selected works showing important breakthroughs on high-quality $Mg_xZn_{1-x}O$ growth can be found in table 1.

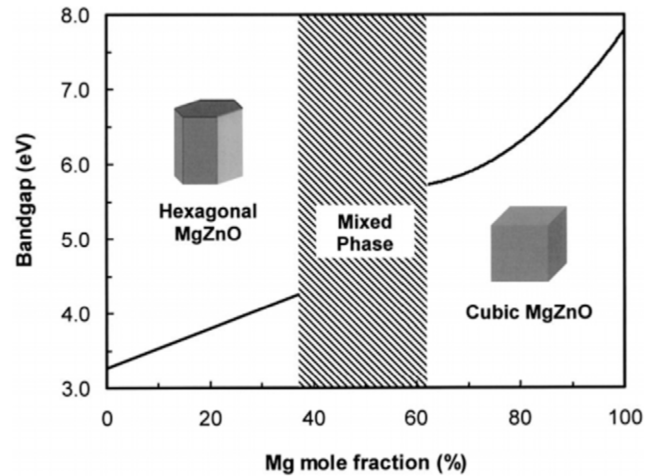

Figure 1. Band-gap energy as a function of Mg content in $Mg_xZn_{1-x}O$ films. The films have wurtzite and cubic crystal structures for Mg composition less than 37% and greater than 62%, respectively. There is a mixed hexagonal and cubic phase for Mg compositions between 37% and 62%. (Reprinted from [32]. Copyright 2003 AIP Publishing LLC).

It should be noted that $Mg_xZn_{1-x}O$ is not the sole compound for band-gap engineering. Other ternary or quaternary alloys based on ZnO, such as $Be_xZn_{1-x}O$, $Ni_xZn_{1-x}O$ and $Be_xMg_yZn_{1-x-y}O$, are also used to tailor the band gap to the deep-UV region [46–49]. Although most of the research still focuses on the optoelectronic properties, a few prototype UV PDs based on these materials have been reported recently [50]. It is predictable that these materials will also be excellent candidates for UV PDs in the future. Considering that there are far fewer reports on the UV PDs fabricated with these materials than with the $Mg_xZn_{1-x}O$ UV PDs, we only representatively reviewed the latter in this paper.

2. Photoconductors

The photoconductor (or photoconductive detector) is the simplest and most primitive PD in device structure. It is configured by depositing a pair of ohmic contacts on a semiconductor thin film, as shown in figure 2. When the incident photon energy exceeds the band-gap energy of the semiconductor, photocurrent will be generated and monitored by external circuits. The strength of the photocurrent signal is closely related to the applied bias and the distance between the electrodes. Therefore, a considerable internal gain could be expected in photoconductors. Assuming the incident light is fully absorbed, the photoconductive gain is expressed by

$$G = (\mu_n + \mu_p)\,\tau E/L = \tau/(t_n + t_p) \qquad (2.1)$$

where μ_n, μ_p, τ, E and L are the electron and hole mobilities, the average carrier lifetime, the strength of the electrical field and the distance between electrodes, respectively. $t_n = L/(E\mu_n)$ and $t_p = L/(E\mu_p)$ are the electron and hole

Table 1. Development of high-quality $Mg_xZn_{1-x}O$ band-gap engineering.

Year	Mg content (%)	Band gap (eV)	Growth technique	Crystal structure	Substrate	References
1998	25		MBE	W	sapphire	[36]
1998	33	3.99	PLD	W	sapphire	[37]
1999	40	4.0	PLD	W	sapphire	[38]
2001	49	4.3	MOVPE	W	sapphire	[39]
2003	51	4.45	MBE	W	sapphire	[40]
2004	51		e-beam	W	sapphire	[41]
2007	44	4.25	MBE	W	sapphire	[42]
2009	55	4.55	MBE	W	sapphire	[33]
2009	55	4.55	MBE	W	sapphire	[34]
2002	50	5.0	PLD	C	sapphire	[43]
2003	47		e-beam	C	sapphire	[44]
2012	30	4.85	MBE	C	MgO	[35]
2005		4.65	MBE	quasi-alloy	sapphire	[45]

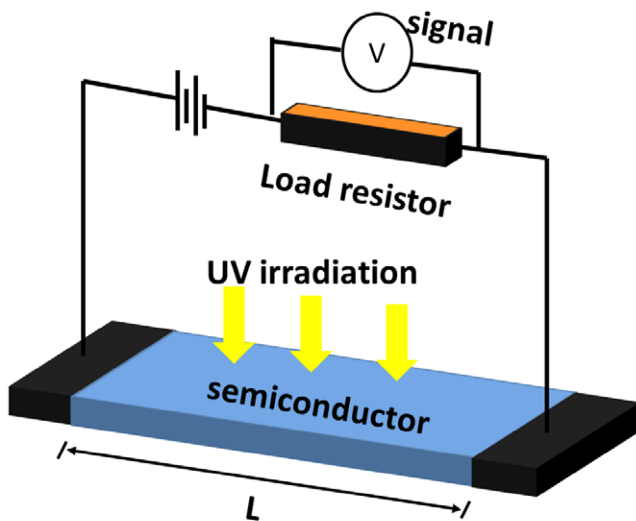

Figure 2. Schematic diagram of a photoconductive PD.

transit times, which indicate the times for carrier transport from one electrode to another. From equation (2.1), large photoconductive gain is available by decreasing the distance between electrodes or increasing the carrier lifetime. It should be noted that long carrier lifetime could demolish the response speed of the UV PD.

2.1. ZnO photoconductors

The energy conversion efficiency of a photoconductor from UV light to electrical signal is strongly related to its ohmic contacts, as a certain amount of photocurrent will be consumed at the contact resistance as Joule heat [51, 52]. As a result, the intensity of the photoresponse signal will be weakened. Therefore, ohmic contacts with low specific resistance on ZnO have been chased extensively by a number of groups on behalf of ZnO-based optoelectronic devices [53]. Up until now, a variety of electrode materials has been developed for ZnO photoconductors, such as Ti/Au, Al/Au, Ni/Au, Al and so on [53].

Besides the contacts, the crystalline quality of ZnO is another main factor which directly dominates the photoresponse properties [54]. Many groups have attempted to improve the ZnO photoconductors by either optimizing growth techniques or applying post-growth treatments. From an early study, Takeuchi *et al* fabricated ZnO-based photoconductors on grained layers grown by the gas evaporation method in an Ar/O_2 ambient. They found that the photosensitivity is improved with ZnO grain size increasing from 7.6 to 40 nm, which was realized by controlling the gas pressure during growth [55]. In the year 2000, Liu *et al* reported a prototype metal–semiconductor–metal (MSM) UV photoconductor with Al contacts fabricated on a semi-polar high-quality single-phase ZnO thin film, which was epitaxially grown on sapphire $(01-12)$ substrate by MOCVD [56]. Ohmic contact was confirmed from current–voltage (I–V) characteristics under both dark and illumination (figure 3(*a*)). The photoconductor shows a distinctive cutoff near 373 nm with a responsivity of 400 A W^{-1}, and a UV/visible rejection ratio of 10^3 at 5 V bias (figure 3(*b*)). The peak responsivity increases linearly with the increasing applied voltage (figure 3(*c*)), indicating an internal gain, and the device has a fast response of 1.5 μs (figure 3(*d*)). Soon afterwards, photoconductors with interdigital (IDT) electrodes were developed by applying Al onto a *c*-plane preferred ZnO thin film, which was fabricated on a quartz substrate by radio frequency (RF) sputtering. The UV PD exhibits a high responsivity of 18 A W^{-1} at 365 nm under 5 V bias [57]. With the same growth method, Liu *et al* fabricated a fast-response IDT ZnO photoconductive detector, whose photoresponsivity achieved 30 A W^{-1} at 360 nm under 3 V, with a rejection ratio of five orders of magnitude [58]. Including growth techniques [59–61], many post-growth treatment techniques have been exploited to further enhance the device performance of ZnO-based photoconductors, such as annealing, surface treatment or device structure design [62–65]. For example, by a post-annealing technique, Bi *et al* found that the photoresponsivity can be massively improved from 0.004 to 2069 A W^{-1} [62].

It is not surprising that response speed is intensively concerned in the ZnO-based UV photoconductors, as a two-step UV response has been observed ever since the early studies [66, 67]. The two-step response consists of a fast and a slow response branch. The former was due to electron–hole generation or recombination, whilst the latter was attributed to oxygen photochemical absorption and desorption of carriers at that time. Obviously, the slow response relates to stoichiometric composition and crystal quality [68]. Because

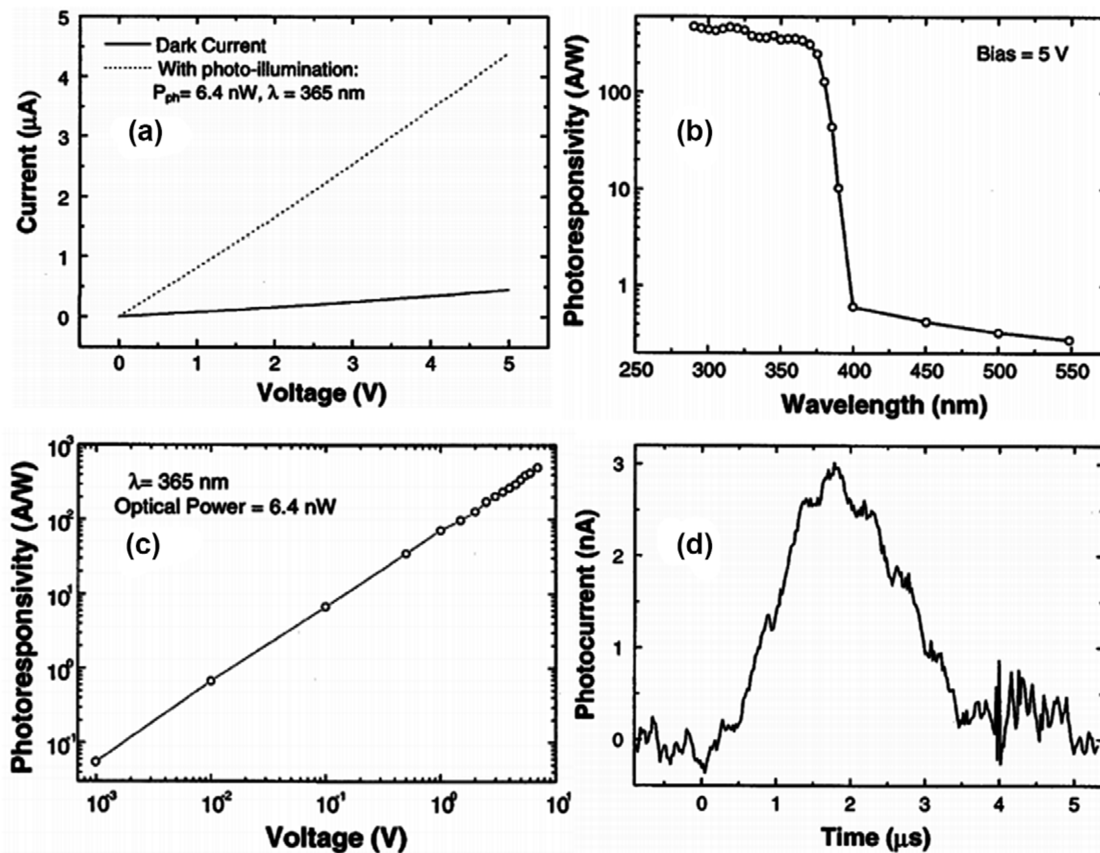

Figure 3. (*a*) Dark (solid line) and photoilluminated (dashed line) current–voltage (I–V) characteristics from a ZnO photoconductor, (*b*) spectral response at 5 V bias, (*c*) photoresponsivity versus bias voltage and (*d*) transient photoresponse of the photoconductor. (Reprinted from [56]. Copyright 2000 Springer).

of the restriction of growth technology, the response speed was always as long as seconds or even several tens of minutes in those days. The limit was broken by the UV photoconductor fabricated on an MOCVD epitaxially grown ZnO film [56]. The detector realized a response time with a rise of 1 μs and a fall of 1.5 μs (figure 3(*d*)). With the RF sputtering method, a fast-responding ZnO UV photoconductor with IDT electrodes was fabricated on a *c*-plane preferred ZnO thin film. From the transient response characterization, a photoresponse speed with rise time of 100 ns and fall time of 1.5 μs was achieved [57]. After improving the quality of the ZnO film by post-growth annealing, the rise time was further shortened to 45 ns, as shown in figure 4 [62]. By the same growth method, Liu *et al* studied an ultra-fast ZnO photoconductor with a rise time of 20 ns [58]. For the photocurrent fall time, a 'fast decay' on the scale of nanoseconds and a 'slow decay' on the scale of microseconds were both observed. According to their calculations, the fast decay is due to the electron transit time between the electrodes, and the slow decay is ascribed to excess lifetime of trapped holes. In the year 2006, Moazzami and Murphy systematically studied the ultra-long-time decay of ZnO by MBE growth [69, 70]. They proposed that the long decay is due to the intrinsic defect induced deep energy levels. By SiO_2 passivation, the long decay time can be extensively cured. An effective way to compensate deep-level intrinsic defects is doping, where Al [71, 72], Ga [73–75], Ag [76] and N [56, 77, 78] are mostly used. Currently, the fastest speed achieved is 10 ns at rise and 960 ns at fall, where the ZnO thin film was doped by 0.7 wt% Ga [74].

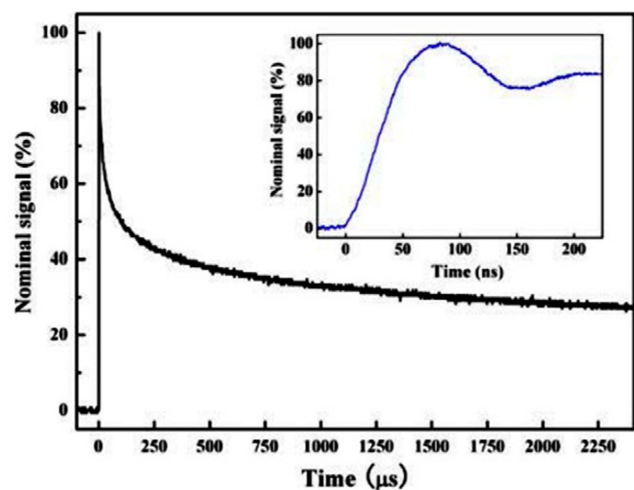

Figure 4. Rise time and decay time of a fast-response ZnO photoconductor. (Reprinted from [62]. Copyright 2008 Springer).

Interestingly, ZnO UV photoconductors based on wet chemical synthesis methods, such as sol–gel and spray pyrolysis, have been attracting more attention than the advanced epitaxial methods in the past few years. The reason

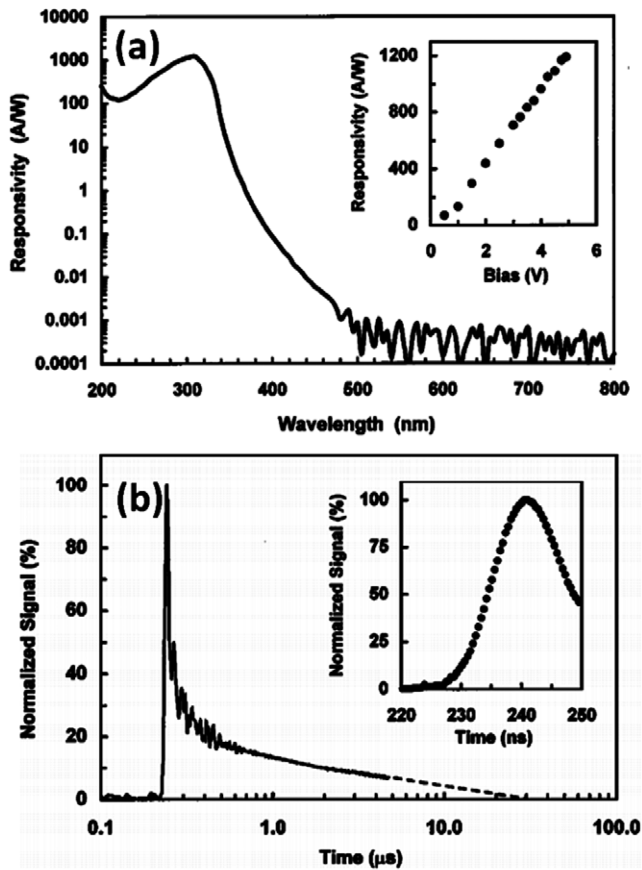

Figure 5. (*a*) Spectral response of a $Mg_{0.34}Zn_{0.66}O$ UV photoconductor biased at 5 V. The inset shows the responsivity as a function of bias voltage under 308 nm, 0.1 mW UV illumination. (*b*) Response speed of the $Mg_{0.34}Zn_{0.66}O$ UV photoconductor biased at 5 V. The inset shows the rise time. (Reprinted from [82]. Copyright 2001 AIP Publishing LLC).

lies in the advantages in the cost as well as the development of ZnO-based flexible electronic devices [79]. For instance, together with the doping method, Shinde and Rajpure demonstrated a spray pyrolysis synthesized ZnO : Al UV photoconductor which has a photoresponsivity of 1125 A W^{-1} under 5 V, comparable to the value of epitaxially grown ZnO UV photoconductors. The detector also possesses a good stability, which was checked by periodic UV illumination [80]. However, the samples synthesized by chemical methods always contain many intrinsic defects. A recent study indicates that such defects can be reduced by doping, which is helpful to increase the response speed [81].

2.2. $Mg_xZn_{1-x}O$ *photoconductors*

The first MgZnO-based UV photoconductor was invented not long after it was proposed as a band-gap-tuneable WBG semiconductor [82]. The device was constructed with Cr/Au IDT electrodes deposited on $W-Mg_{0.34}Zn_{0.66}O$ epitaxial film grown by PLD. The PD possesses a high photoresponsivity of 1200 A W^{-1} with a fast response of 8 ns rise time and 1.4 μs fall time, and a UV/visible light rejection ratio over four orders of magnitude (figure 5). The cutoff wavelength is 317 nm, much shorter than that of ZnO photoconductors (375 nm). A sub-band response tail was observed from the spectrum response, which the authors attributed to the Mg content fluctuation (figure 5). Good progress has been made on deep-UV photoconductors based on C-MgZnO as well. The cutoff wavelength can be adjusted from 157 to 230 nm, leaving an unexploited gap between 4.28 and 5.51 eV at that time [32]. Han *et al* demonstrated a photoconductive solar-blind deep-UV PD with Au IDT electrodes fabricated on a $C-Mg_{0.52}Zn_{0.48}O$ film (figure 6(*a*)), which is grown on lattice-matched MgO substrate by MOCVD [83]. The ohmic contacts were confirmed with I–V characterization (figure 6(*b*)). The detector shows a peak responsivity of 273 mA W^{-1}, with a sharp cutoff at 253 nm and a rejection ratio of about four orders of magnitude (figure 6(*c*)). A relatively long decay time of 1.6 μs was observed (figure 6(*d*)), which is attributed to the hole-trap effect of surface oxygen vacancies. As well as the aforementioned PLD and MOCVD methods, RF sputtering [84, 85], MBE [86] and even sol–gel [87] growth methods have been exploited for fabrication of $Mg_xZn_{1-x}O$ UV photoconductive detectors. It is noticeable that the response speed of $Mg_xZn_{1-x}O$ UV photoconductors is much faster than that of ZnO ones, which is probably due to the compensation of intrinsic hole-trapping deep-level defects (Zn interstitial and O vacancies) by Mg ions.

As the resistivity of $Mg_xZn_{1-x}O$ is much higher than that of ZnO, research on $Mg_xZn_{1-x}O$ UV photoconductors always involves the study of the noise or internal gain. Yang *et al* discovered that the shot noise dominates the detector instead of Johnson and $1/f$ noise if the operating frequency is not too low [82]. By using an MOCVD-grown film, Zhao *et al* demonstrated a photoconductor with maximum responsivity of 14.62 A W^{-1} at 340 nm, with a UV/visible rejection ratio of more than two orders of magnitude and a fast response speed of 400 ns [88]. The NEP of the detector is 2.19×10^{-11} W $Hz^{-1/2}$, which generates a normalized detectivity of 2.68×10^7 cm $Hz^{1/2}$ W^{-1} at room temperature. Further, Jiang *et al* developed a MgZnO UV photoconductor with a low noise level on a $W-Mg_{0.4}Zn_{0.6}O$ film prepared by RF sputtering. The responsivity of the detector is about 1.3 A W^{-1} at 320 nm under 3 V bias, with a UV/visible rejection ratio of more than four orders of magnitude and a quantum efficiency more than 505%. As the NEP of the detector is very low, the device possesses a high normalized detectivity of 1.37×10^{11} cm $Hz^{1/2}$ W^{-1}, which is higher than that of GaN UV photoconductive detectors [85]. Internal gain was also tentatively studied within $Mg_xZn_{1-x}O$ based UV photoconductors. It is revealed that hole lifetime, prolonged by hole traps at the electrode/MgZnO interface, plays an important role apart from the photoconductive gain [83]. This is similar to the aforementioned situation of ZnO-based photoconductors.

3. Schottky and MSM photodiodes

Schottky photodiodes based on WBG semiconductors have been used for UV detection for many years because of their easy fabrication, low noise and high response speed. According to Schottky–Mott theory, the Schottky barrier can be given by

$$\Phi_{ms} = \Phi_m - \chi_s \qquad (3.1)$$

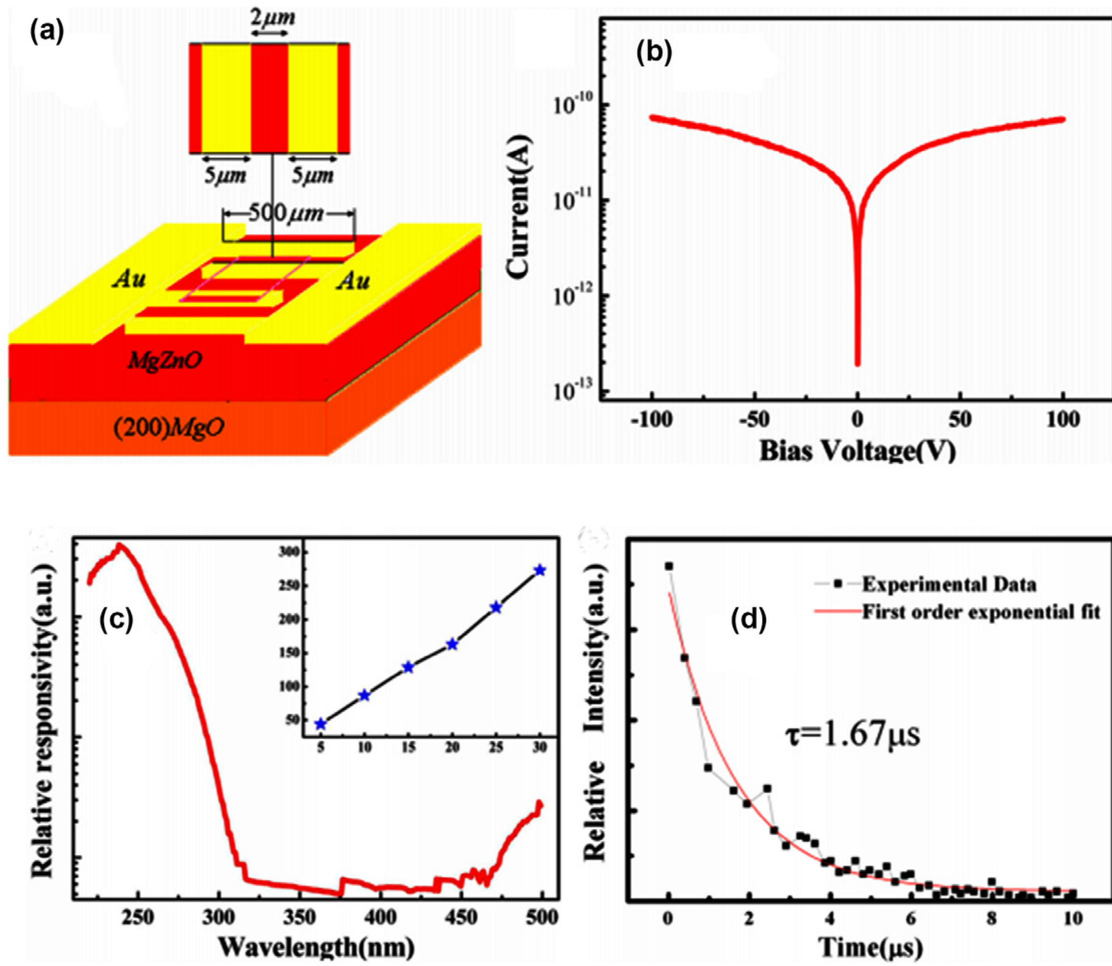

Figure 6. (*a*) Schematic illustration of $Mg_{0.52}Zn_{0.48}O$ photoconductor with IDT electrodes, (*b*) the I–V characteristic, (*c*) the spectral response at 15 V bias voltage and (*d*) the temporal pulse response of the $Mg_{0.52}Zn_{0.48}O$ UV photoconductor. (Reprinted from [83]. Copyright 2011 AIP Publishing LLC).

where Φ_{ms}, Φ_m and χ_s are the height of the Schottky barrier between a metal and a semiconductor, the work function of metal contacts and the electron affinity of a semiconductor. For a Schottky junction, the current is basically dominated by the majority carriers. The current density can be expressed as under the thermal emission model [89]

$$J = J_0 \left[\exp\left(\frac{qV}{nKT}\right) - 1 \right] \qquad (3.2)$$

and

$$J_0 = A^* T^2 \exp(-q\phi_{ms}/kT) \qquad (3.3)$$

where J_0, V, k, n, T and A^* are the inverse saturation current, applied voltage, Boltzmann constant, ideality factor, absolute temperature and Richardson constant, respectively. Due to the existence of surface states in ZnO and related materials, equation (3.1) could no longer be used to accurately estimate the Schottky barrier height. Instead, equations (3.2) and (3.3) can be used for fitting the I–V curve in order to determine the ideality factor and barrier height. Usually, the Schottky barrier height of ZnO (or $Mg_xZn_{1-x}O$) based Schottky photodiodes is large, as well as the built-in electrical potential, which is defined as $qV_{bi} = \Phi_m - \Phi_s$($\Phi_s$ is the work function of a semiconductor). Even under zero external bias, the photogenerated electron–hole pairs can still be collected by the electrodes due to such built-in electrical field, known as the 'photovoltaic mode'.

Schottky-type IDT MSM photodiodes are widely used in practical optoelectronics circuits, especially for optoelectronic communication and signal processing circuits. The MSM photodiode is composed by a pair of back-to-back Schottky contacts, as shown in figure 7(*a*). One of the Schottky contacts will be reverse biased and the other forward biased when the MSM photodiode is working. A typical I–V curve of an MSM photodiode is shown in figure 7(*b*). The current increases and then saturates from low to high bias voltage, which is due to the expansion of the depletion region of the reverse biased contact and the flat-band effect of the forward biased contact, respectively [20]. Figure 7(*c*) schematically shows the band structure of the MSM photodiodes under equilibrium and working conditions, respectively. There are several obvious advantages of MSM photodiodes:

(a) low stray capacitance, which allows the application in high-frequency circuits;
(b) avoid the severe UV light absorption by the metal electrodes compared to the Schottky photodiode;

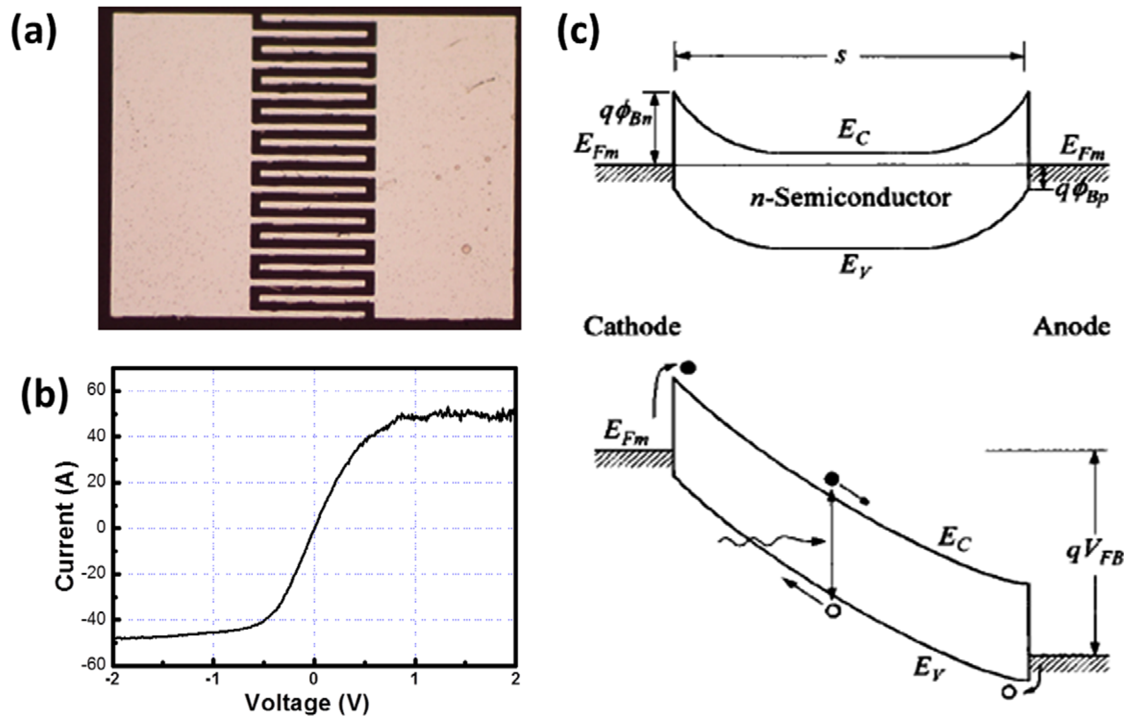

Figure 7. (*a*) A $Mg_xZn_{1-x}O$ MSM photodiode with Ag IDT electrodes, (*b*) a typical I–V curve of a Ag–$Mg_xZn_{1-x}O$ Schottky-type IDT MSM photodiode and (*c*) the band structure of the MSM photodiodes under equilibrium and working conditions. ((*c*) reprinted from [20]. Copyright 2006 John Wiley and Sons).

(c) the planar structure is compatible with the FET and TFT structure for integrated circuit chips;
(d) internal gain has been discovered on WBG semiconductor MSM photodiodes.

3.1. ZnO Schottky and MSM photodiodes

3.1.1. ZnO Schottky UV photodiodes. ZnO Schottky contacts have been widely reported, as they are essential for developing ZnO optoelectronics [90]. Research on Schottky photodiodes also has made huge progress in accordance. It is a key issue to improve the quality of Schottky contacts to promote the performance of a photodiode. The methods include improving the thin-film quality, metal selection and surface passivation/treatment before the contact fabrication [53, 91, 92].

As early as 1986, the Au Schottky contact was applied on sputtered polycrystalline ZnO film to form a UV photodiode [25]. However, the quantum efficiency and response speed are poor, which was attributed to the low crystal quality of the thin film. This argument has been proved by a study of post-growth annealing effects on ZnO Schottky photodiodes [93]. A post-growth annealing of PLD-deposited ZnO film was conducted at 400, 500, 600, 700 and 800 °C for 1 h in air. After annealing, the crystallinity and uniformity were indeed found to be improved. Among them, the sample annealed at 600 °C is the best one regarding both the optical properties and stoichiometric ratio, as shown in figure 8(*a*). The Pt/ZnO Schottky photodiode fabricated on 600 °C annealed film has the highest barrier height of 0.8 eV with the lowest reverse leakage current of 1.5×10^{-5} A cm^{-2} (figure 8(*b*)). Compared to the other photodiodes, the one fabricated on 600 °C annealed ZnO film also shows the largest responsivity of 0.265 A W^{-1} under UV illumination (figure 8(*c*)), and the fastest photoresponse component, with a rise time of 10 ns and a fall time of 17 ns (figure 8(*d*)). A recent comparative study of the Pd/ZnO Schottky photodiode shows similar results [94]. The ZnO thin films were synthesized by the vacuum thermal evaporation and sol–gel methods, respectively. From comparison of the XRD results, the latter thin film shows a better crystallinity than the former. As a result, the quantum efficiency, responsivity and rejection ratio of the Schottky photodiode fabricated on sol–gel synthesized ZnO film are higher than those of the other one.

ZnO Schottky contacts formed by different metals have different barrier heights and ideality factors, which significantly affect the photoresponse performance of the device. Metals with high work function are frequently employed to acquire large barrier height to achieve a low dark current. By applying Au contacts to a ZnO film epitaxially grown by MBE, Oh *et al* constructed a band-pass UV photodiode from 195 to 380 nm with a low dark current of $\sim 10^{-8}$ A and a large current build-up of $\sim 10^3$ under UV illumination [95]. Young and co-workers reported an Ir/ZnO Schottky UV photodiode fabricated by RF sputtering [96]. The reverse current is as low as 8.87×10^{-11} A, indicating a low noise level of the photodiode. The responsivity is 10 mA W^{-1}, with a rejection ratio of 4.6×10^2 at -1 V. As metal contacts are opaque or semi-transparent to UV light, Schottky UV photodiodes with transparent electrodes have been receiving more and more attention recently due to their large optically active area. A transparent PEDOT : PSS polymer electrode fabricated on commercial Zn-polar ZnO

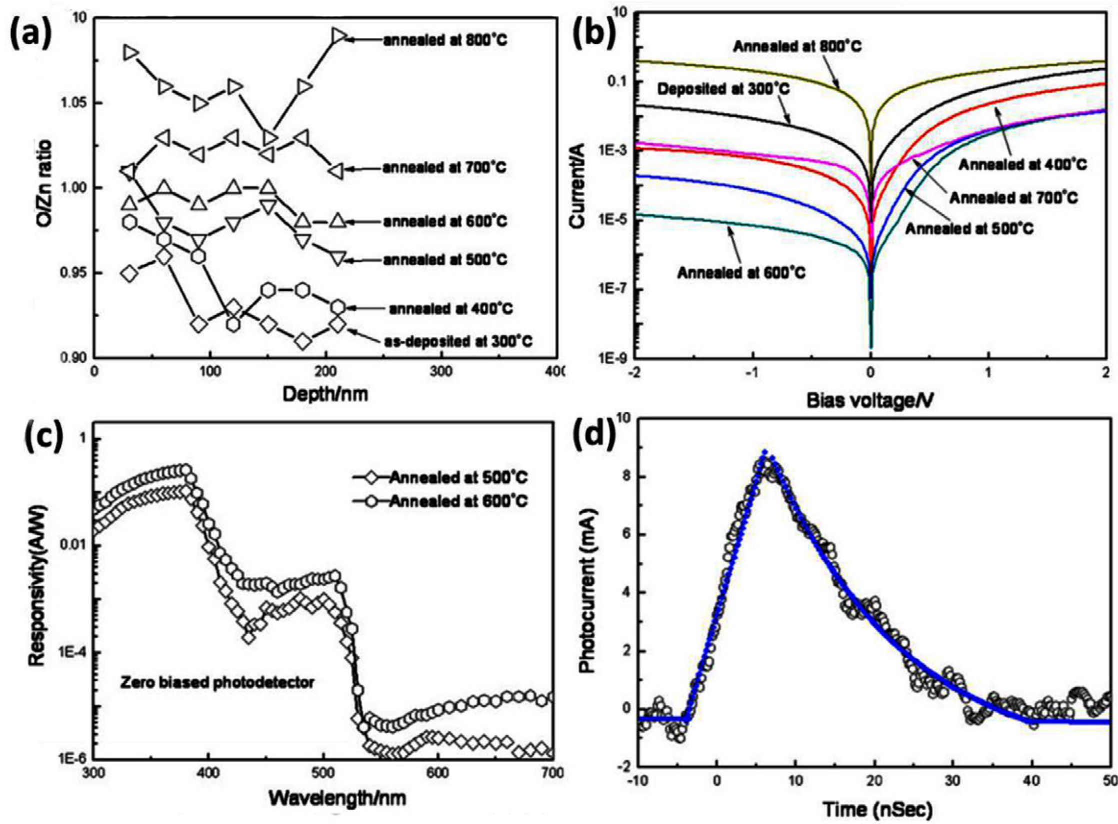

Figure 8. (*a*) O/Zn ratio as a function of depth from ZnO film surface of the films annealed at different temperatures, (*b*) dark I–V curves of the Schottky photodiodes fabricated on ZnO films with Pt electrodes, (*c*) the photoresponse spectra of Schottky photodiodes fabricated on the ZnO films annealed at 500 and 600 °C and (*d*) photocurrent as a function of response time of PD. (Reprinted from [93]. Copyright 2011 Elsevier).

substrate was first reported, with a high barrier height of 1.1 eV and an ideality factor of 1.02, by Nakano *et al* [97]. The PD has an ultralow dark current of $\sim 10^{-12}$ A (figures 9(*a*) and (*b*)), a high responsivity of 0.2 A W^{-1} in photovoltaic mode a with rejection ratio of 10^3 (figure 9(*c*)), and a high detectivity of 2.4×10^{14} cm $Hz^{1/2}$ W^{-1} at 280 nm, which is comparable to the best result of AlGaN p–i–n PDs. Inorganic transparent Schottky electrodes are also developed for UV PDs. For example, Ag_xO and Pt_xO electrodes have been applied on a ZnO film grown by PLD [98]. In photovoltaic mode, the highest responsivity achieved was 0.1 A W^{-1}, with a detectivity of 1.29×10^{11} cm $Hz^{1/2}$ W^{-1}.

Surface states are another factor to consider for the Schottky UV PDs, as they can either change the Schottky barrier height by Fermi level pinning or act as carrier transport channels [20]. To increase S/N ratio by reducing the influence from surface states, several strategies have been taken into consideration, such as novel design of device structures, surface treatment and so on. By inserting a 5 nm SiO_2 layer between the ZnO film and Cr/Au electrodes, Ali and Chakrabarti obtained a relatively high rejection ratio with sol–gel synthesized ZnO thin film [99]. Further, they also systematically studied the effect of thermal treatment on Cr/Au–ZnO Schottky UV photodiodes [100]. The electrodes were annealed in an oven from 50 to 300 °C. It was found that the Schottky barrier height does not change much throughout the whole temperature scale. However, the ideality factor decreases, then stays at a constant value and finally increases drastically when the annealing temperature changes from 50 °C to 100 °C, between 100 °C and 200 °C, and over 200 °C, respectively. Accordingly, the rejection ratio of the photodiode increases at the beginning then stays at a constant value, and finally decreases dramatically, indicating an obvious change of the device performance under different annealing temperatures. The effect of the annealing process on device performance was interpreted as follows. At low temperature, the undesirable surface states of OH^- bonds are suppressed and grain size becomes larger, thus the device performance is improved. At high temperature, degradation of the photodiode results from interfacial reactions of Cr and ZnO, and the phase transitions of the chromium oxide during annealing. Apart from this, the Schottky barrier height is sensitive to the polarity of ZnO. It has been proved that Pt/Zn-polar ZnO has a larger barrier height, a better ideality factor, a lower inverse saturation current and a higher responsivity than Pt/O-polar ZnO [101].

3.1.2. ZnO MSM photodiodes The ZnO MSM UV photodiode was presented soon after the Schottky photodiode and has been studied quite extensively from then on, due to its predominant merits mentioned earlier. A number of growth approaches have been exploited to prepare high-quality ZnO thin film for MSM UV photodiodes, including MOCVD [54], MBE [102–106], PLD [107], ALD [108] and sputtering [109–114]. Liang *et al* designed a Ag–ZnO–Ag MSM photodiode on an epitaxial film grown by MOCVD

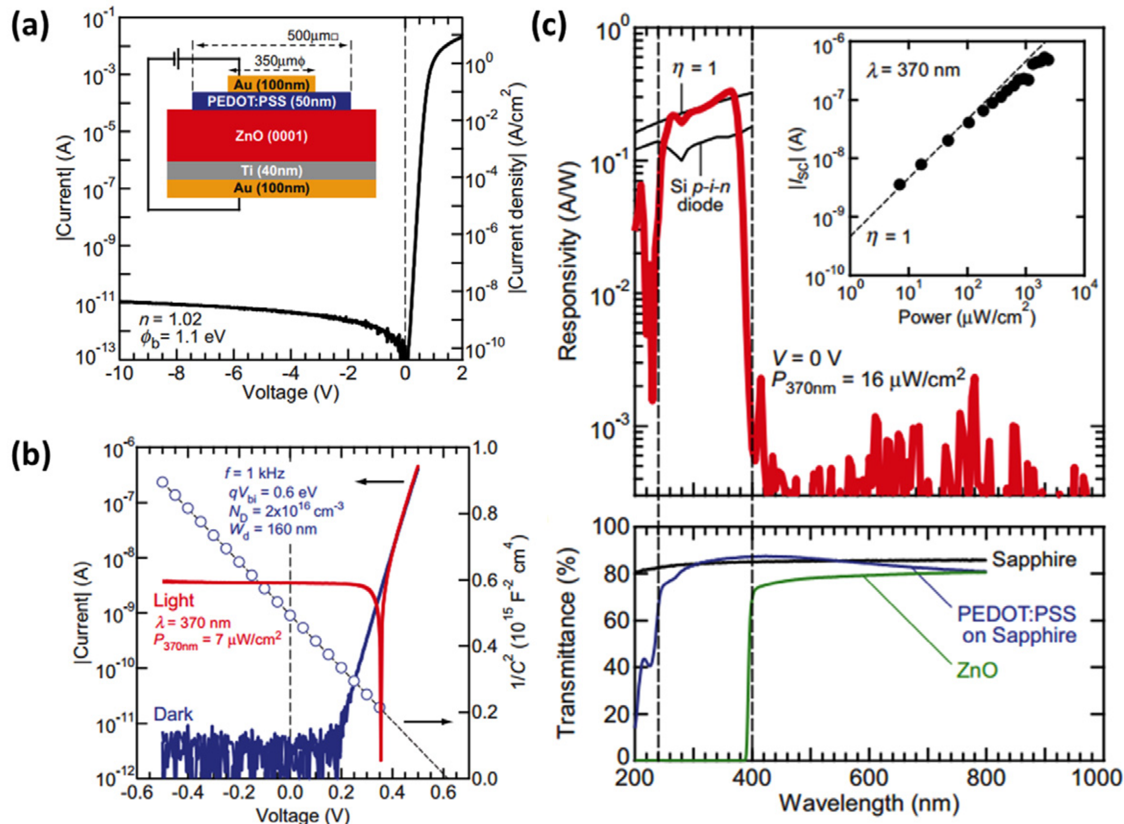

Figure 9. (a) A typical I–V characteristic of the PEDOT:PSS/ZnO Schottky photodiode under dark conditions. The ideality factor (n) and the Schottky barrier height (ϕ_b) are also shown. The inset shows a schematic cross section of the PEDOT : PSS/ZnO Schottky photodiode. (b) The I–V (blue curve) and the $1/C^2$–V (blue open circles) characteristics under dark conditions and the I–V characteristic (red curve) under illuminated conditions. (c) The spectral response of the PEDOT : PSS/ZnO Schottky photodiode at $V = 0$ V (top panel), and transmission spectra of sapphire, a 50 nm thick PEDOT : PSS thin film on sapphire and ZnO single-crystal substrate (bottom panel). (Reprinted from [97]. Copyright 2008 AIP Publishing LLC).

in 2001 [54]. The barrier height is estimated as 0.84 eV using an Ag–ZnO–Al Schottky structure (figure 10(a)). The dark current is five orders of magnitude smaller than the photoconductive counterpart (figure 10(b)). The photoresponsivity of the MSM photodiode is 1.5 A W^{-1} at 5 V (figure 10(c)), with a fast response speed of 12 ns for the rise time, and 50 ns for the fall time (figure 10(d)). Young *et al* studied an MSM UV photodiode fabricated on MBE-grown ZnO with Ru electrodes, with the barrier height of 0.71 eV. The dark current and contrast ratio are 8×10^{-8} A and 225, respectively. From the transient response measurement, a time constant of 13 ms was obtained, much faster than that of ZnTe counterparts [102]. They also studied an MSM UV photodiode with Pd electrodes with a similar barrier height to Pd/ZnO. The detectivity of the MSM photodiode is as high as 6.25×10^{11} cm $Hz^{1/2}$ W^{-1} [104]. Apparently, the performance of ZnO MSM photodiodes fabricated by MBE is worse than that by MOCVD, which is probably due to the different intrinsic defects in the film introduced by different growth processes, or the defects at the electrode/ZnO interface introduced by the device fabrication processes. By RF sputtering, Jiang *et al* researched an Au–ZnO–Au MSM photodiode with a low dark current of 1 nA at 3 V [109]. The detector has a photoresponsivity of 0.337 A W^{-1} at 3 V with a high UV/visible rejection ratio of more than four orders of magnitude. The 10–90% response time is as fast as 20 ns in rise and 250 ns in fall. Moreover, it is discovered that the transient response is independent of the distance between the electrodes, which means the transit time of the carriers cannot be the primary contribution to the response time. Ultimately, the response speed was attributed to trapping of holes. It is worth mentioning that other methods apart from epitaxial growth, such as thermal oxidation, are also adopted to synthesize ZnO thin films for UV MSM photodiodes [115]. The performance of such ZnO UV MSM photodiodes is even comparable to those fabricated by the epitaxial method [115].

Similarly to Schottky photodiodes, large Schottky barrier height is helpful to reduce the dark current and enhance the S/N ratio of the UV MSM photodiodes. Li *et al* comparatively studied MSM photodiodes with Au and Cr electrodes fabricated on PLD-grown ZnO films [107]. As the work function of Au is much larger than that of Cr, the barrier of Au–ZnO is higher than that of Cr–ZnO. The dark current of the Au–ZnO–Au MSM photodiode turns out to be three orders of magnitude lower than that of the Cr–ZnO–Cr MSM detector. A similar study has been carried out on MBE-grown ZnO MSM photodiodes with Ag, Pd and Ni electrodes [103]. The Schottky barriers were estimated as 0.736 eV, 0.701 eV and 0.613 eV for Ag–ZnO, Pd–ZnO and Cr–ZnO contacts, respectively. The dark current of the Ag–ZnO MSM

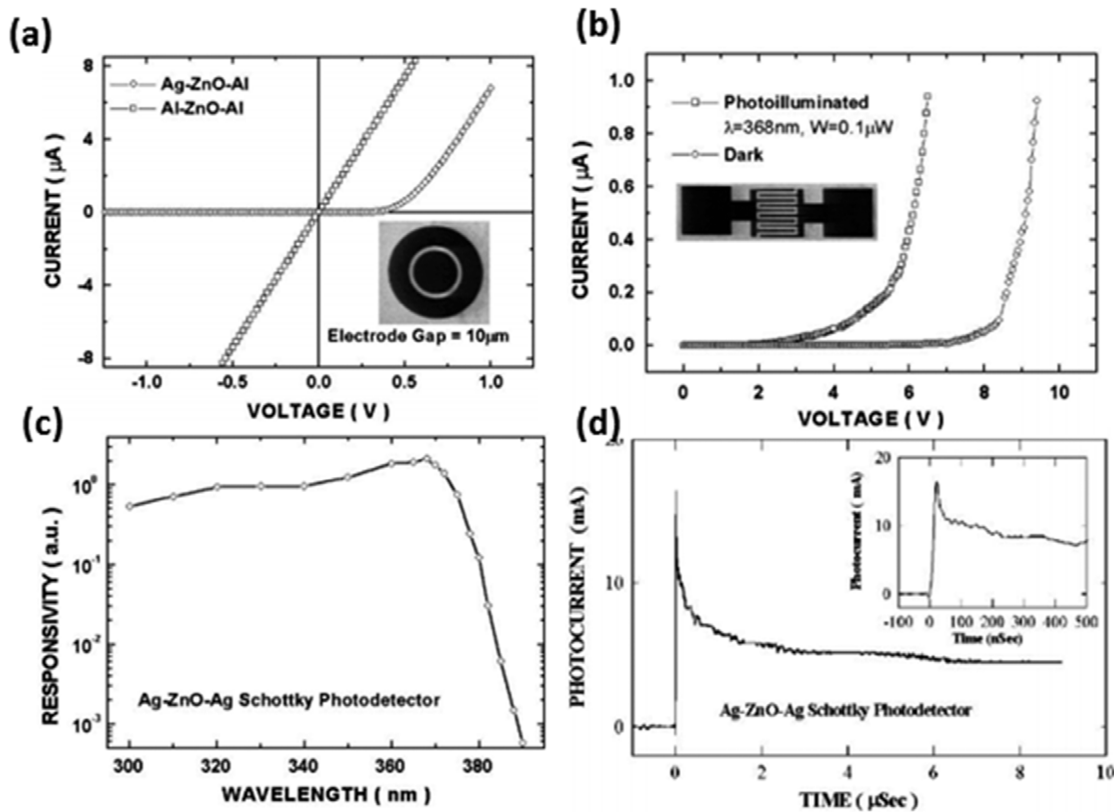

Figure 10. $(a)\,I$–V characteristics of ZnO Schottky diodes. $(b)\,I$–V characteristics of a ZnO Schottky PD with Ag IDT electrodes. The inset shows an SEM picture of the top view of the device. (*c*) Spectral photoresponse of a ZnO Schottky PD. (*d*) Photocurrent as a function of response time of the ZnO MSM PD. (Reprinted from [54]. Copyright 2001 AIP Publishing LLC).

photodiode is the lowest among the three (Ag, 2.9×10^{-9}, Pd, 1.19×10^{-8} and Ni, 2.45×10^{-7} A, at 1 V), with the highest UV/dark rejection ratio (figures 11(*a*) and (*b*)). The low-frequency noise of the MSM photodiode with Ag electrodes is almost one order smaller than that of the other two due to its much lower dark current. Similar results can also be found in other investigations on ZnO MSM photodiodes with Al, Cr and Pd electrodes on an RF sputtered film [110]. To further increase the effective barrier height, an insulating layer is applied in between the ZnO and the contacts to form a metal–insulator–ZnO–insulator–metal (MISIM) geometry. By inserting a 5 nm SiO_2 layer by plasma-enhanced chemical vapour deposition (PECVD), a Pt–SiO_2–ZnO–SiO_2–Pt photodiode was studied. Compared to the Pt–ZnO–Pt photodiode, the dark current can be reduced from 4.11×10^{-7} to 2.22×10^{-10} A at 5 V, and the UV/visible rejection ratio improved from 2.4×10^2 to 3.8×10^3 [105]. As the SiO_2 layer was deposited by a post-growth method, some interfacial defects could be introduced. Yu *et al* developed a Au–MgO–ZnO–MgO–Au MISIM photodiode [111], where the ZnO(0 0 0 1) and MgO(1 1 1) were grown by RF sputtering. The photodiode can work in avalanche mode, with a high responsivity of 1.7×10^4 A W^{-1} and an avalanche gain of 294 at 73 V.

The gain of the ZnO MSM photodiodes has been observed by several groups [54, 106, 109, 115, 116], although the origin is still controversial. Early study shows a gain of 2.5 at 5 V bias in a Ag–ZnO–Ag MSM photodiode [54]. The photoconductive effect at high field was believed to contribute to this gain. Jiang *et al* found the carrier transit time scarcely changes with the distance between the electrodes, thus the photoconductive gain is excluded according to equation (2.1) [109]. They proposed that the gain is relating to the trapping of holes. Later, a high gain of 435 at 3 V in Pd–ZnO–Pd photodiodes was also achieved, where the authors regarded the reason as the presence of oxygen-related hole-trap states at the thin-film surface [115]. Further, Liu *et al* demonstrated a Au–ZnO–Au photodiode with a super-high responsivity of 26 000 A W^{-1} at 8 V (figure 12), corresponding to an internal gain of 9×10^4. The large internal gain of this photodiode is ultimately attributed to the trapping of holes at the metal/ZnO interface [106].

Some novel ZnO-based MSM photodiodes have also been proposed by integrating the photodiodes with underlying substrates/structures. By constructing ZnO MSM photodiodes on poly(ethylene terephthalate) (PET) substrate with a ZnO capping layer deposited by RF sputtering, a flexible UV ZnO–Ag–ZnO–PET photodiode was obtained with a responsivity of 3.80×10^{-2} A W^{-1} at 3 V, and a UV/visible rejection ratio of 1.56×10^3 [117]. Without the capping layer, the responsivity is found to be only 2.36×10^{-3} A W^{-1}. By dc sputtering, another work demonstrated a flexible Pd–ZnO–Pd photodiode fabricated on polypropylene carbonate substrates with a maximum responsivity of 1.59 A W^{-1} [113, 114]. Lee *et al* invented a kind of resonant cavity enhanced MSM UV PD by growing ZnO on a SiO_2/HfO_2 distributed Bragg reflector (DBR) substrate with vapour cooling condensation system [118]. Compared to the conventional ZnO MSM photodiodes, a higher responsivity with a lower noise can be

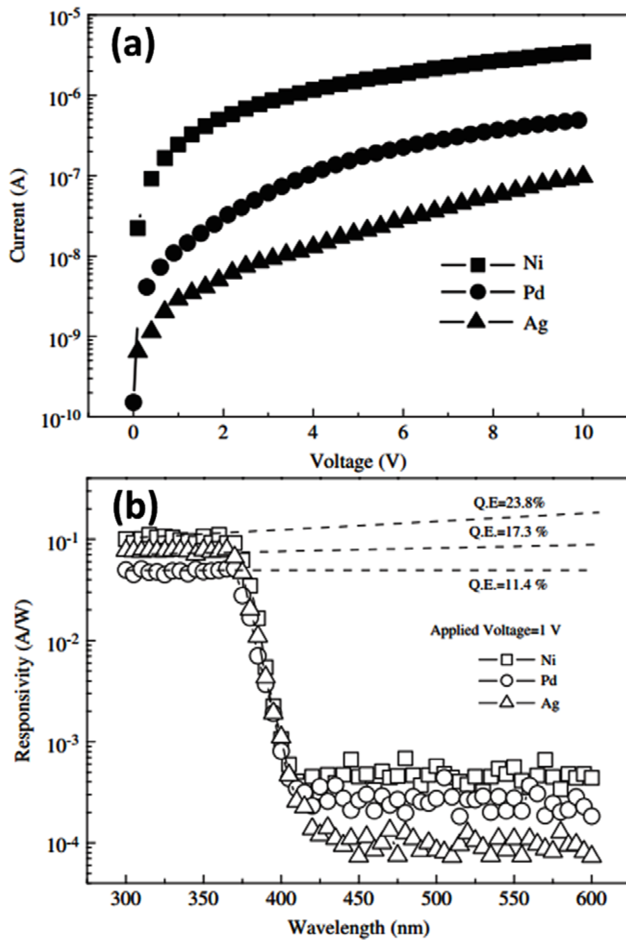

Figure 11. (a) Dark I–V characteristics of ZnO MSM UV photodiodes with Ag, Pd and Ni electrodes. (b) Spectral responsivity of ZnO MSM UV sensors with different electrodes. (Reprinted from [103]. Copyright 2006 AIP Publishing LLC).

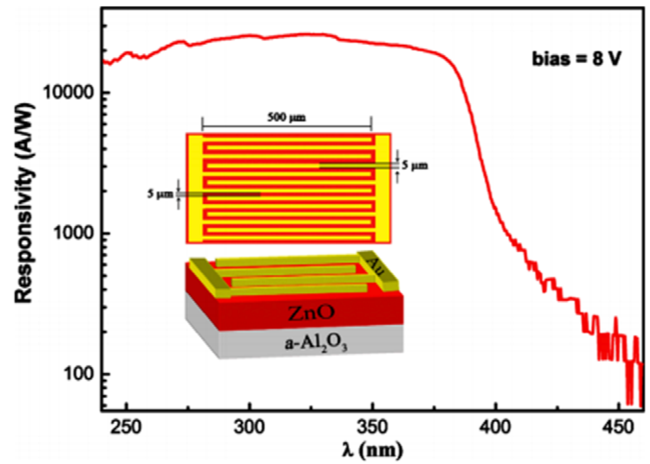

Figure 12. The super-high responsivity of 26 000 A W^{-1} of a ZnO MSM UV detector. (Reprinted from [106]. Copyright 2010 AIP Publishing LLC).

realized with the DBR-MSM photodiode. Moreover, the peak response wavelength can be adjusted via designing a resonant DBR structure beneath, suggesting a new method to realize wavelength-selective UV PDs.

3.2. $Mg_xZn_{1-x}O$ *Schottky and MSM photodiodes*

3.2.1. $Mg_xZn_{1-x}O$ *Schottky photodiodes.* Deep-UV Schottky photodiodes have been achieved based on $Mg_xZn_{1-x}O$ with different x values by either homo- or heteroepitaxial methods [119–125]. By homoepitaxy on ZnO substrate, phase segregation can be efficiently suppressed as aforementioned. Nakano *et al* have successfully grown W-$Mg_xZn_{1-x}O$ on a Zn-polar ZnO substrate, with the x value varying continuously from 0% to 43% [119]. The UV photodiodes based on these epitaxial films were fabricated with PEDOT : PSS Schottky electrodes. The shortest cutoff wavelength is 315 nm, falling in the UV-B region. At the same time, Endo *et al* reported a deep-UV Schottky photodiode with Pt Schottky electrodes, which were fabricated on a W − $Mg_xZn_{1-x}O$ film with the band gap of 4.4 eV grown on ZnO by RF sputtering [120]. The I–V characterization result shows a low leakage current (<1 nA at 30 V) and high breakdown voltage (40 V) (figure 13(a)). The responsivity is 0.034 A W^{-1} at 250 nm in the UV-C region, with a UV/visible rejection ratio more than 10^4 (figure 13(b)). However, the photoresponse from ZnO substrate is difficult to avoid for the homoepitaxially grown samples (inset of figure 13(b)). Therefore, a Schottky photodiode based on heteroepitaxial films is still concerned in spite of the large strain induced by the lattice mismatch, for example 18.3% between ZnO and c-plane sapphire. Prototype deep-UV Schottky photodiodes have been demonstrated on W − $Mg_xZn_{1-x}O$ with x varying from 46% to 56% grown on a-plane sapphire [121]. The absorption edge locates at 4.6 eV (Mg content 56%), with the corresponding UV/visible rejection ratio of 10^6. These results prove that high-performance Schottky-type deep-UV photodiodes can be fulfilled with heteroepitaxial W − $Mg_xZn_{1-x}O$ films.

Due to the difference in chemical properties between Mg and Zn atoms, as-grown $Mg_xZn_{1-x}O$ always suffers from intrinsic strain, stacking fault and interstitial Mg atom problems. Thermal annealing is an effective way to decrease such defects and further improve the quality of the epitaxial film. Han *et al* studied a two-step annealing approach on a W − $Mg_{0.27}Zn_{0.73}O$ thin film grown at 400 °C by MOCVD [122]. The dark current of the photodiode decreased drastically when the as-grown film was annealed at 700 °C in vacuum followed by in air, and a much sharper cutoff was observed, with a UV/visible rejection ratio of 10^4. Such improvement of the performance was ascribed to the decrease of grain boundary density during vacuum annealing and the repair of defects during subsequent annealing in air.

Gain has also been observed within $Mg_xZn_{1-x}O$ based UV Schottky photodiodes, though it was believed to be impossible in a common Schottky photodiode [20]. Tabares *et al* systematically studied the gain mechanism of Au/W − $Mg_xZn_{1-x}O$ Schottky photodiodes with x from 5.6% to 18% [123]. The photodiodes cover the spectral region from 3.35 to 3.48 eV, with UV/visible rejection ratio up to ∼10^5 and responsivity as high as 185 A W^{-1}, indicating a large internal gain. The internal gain performs as a function of the incident photon flux, which is believed to be due to the tunnelling-dominated saturation current at

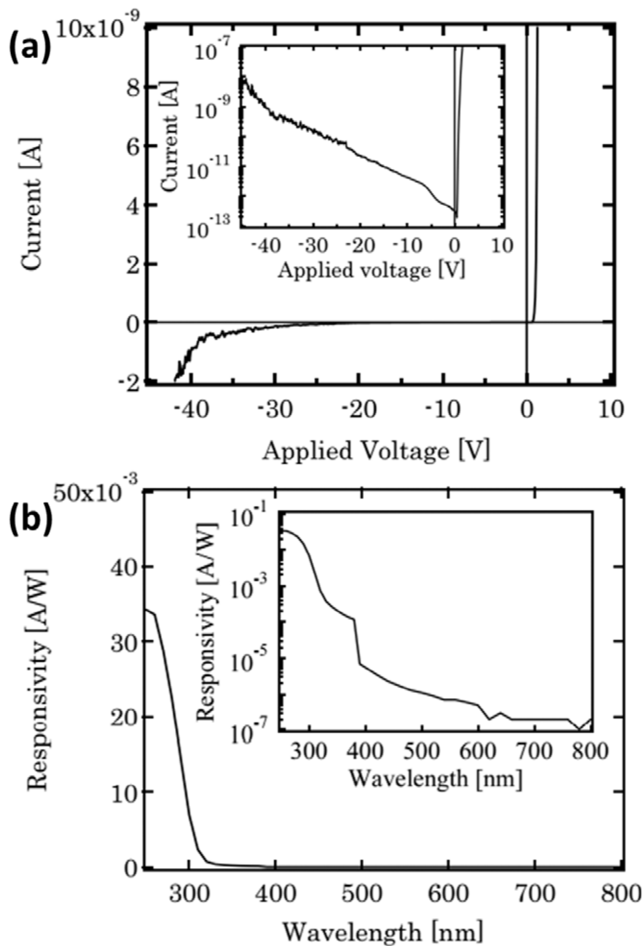

Figure 13. (a) I–V characteristics of the Pt/$Mg_xZn_{1-x}O$ Schottky photodiode on a ZnO single-crystal substrate. The inset shows the I–V characteristics on a logarithmic scale. (b) Photoresponsivity of the Pt/$Mg_xZn_{1-x}O$ Schottky photodiode on a ZnO single-crystal substrate. The inset shows the logarithmic scale of photoresponsivity characteristics. (Reprinted from [120]. Copyright 2008 John Wiley and Sons).

specific bias under illumination. By inserting a thin MgO insulating layer between the Schottky electrodes and the epitaxial film, a UV PD with Au/MgO/W-$Mg_{0.18}Zn_{0.87}O$ structure was constructed [124]. The photodiode possesses a responsivity of 0.55 A W^{-1} at −5 V and a high detectivity of 1.26 × 10^{13} cm $Hz^{1/2}$ W^{-1}, while the responsivity of the controlled photodiode (without MgO insulating layer) is only 6 × 10^{-4} A W^{-1}. The improved responsivity was attributed to the carrier multiplication process occurring in the MgO layer via impact ionization, which interprets the gain mechanism. Further, a Mott-type photodiode with large internal gain was fabricated with a Au/C-MgZnO : Ga/W-MgZnO structure [125]. An external quantum efficiency of the photodiode of 165% was achieved at 30 V bias. The internal gain was ascribed to the electron injection over a reduced Mott potential barrier at the metal–semiconductor interface.

3.2.2. $Mg_xZn_{1-x}O$ *MSM photodiodes.* Intensive investigations have been carried out on MSM UV photodiodes based on W-$Mg_xZn_{1-x}O$, considering the obvious advantages in device structure and practical applications. To flexibly adjust Mg content for UV detection in a broad wavelength range, non-equilibrium growth methods are adopted to overcome the limitation of equilibrium solubility of MgO in ZnO, which is less than 4 mol% from the MgO–ZnO phase diagram [126]. Normally, the substrates used for non-equilibrium growth include sapphire, Si, ZnO and quartz.

Most of the $Mg_xZn_{1-x}O$ MSM photodiodes have been constructed on sapphire substrate up to now. In the year 2003, Takagi *et al* reported a prototype MSM photodiode with Au (5 nm)/Cr (15 nm) electrodes on W − $Mg_{0.5}Zn_{0.5}O$. The epitaxial film was prepared on an *a*-plane sapphire (11−20) substrate by MBE [40]. A peak responsivity of 0.37 A W^{-1} was achieved under 5 V bias with a UV/visible rejection ratio of 3 × 10^3. At the same time, Takeuchi *et al* demonstrated a kind of multichannel MSM photodiode on one chip with gradually increasing Mg distribution by a unique PLD growth on sapphire substrate [127]. The peak responsivity varies from 380 to 288 nm with Mg fraction from 0% to 38%, with a typical response speed of 8 ns. In the higher Mg content region, a phase segregation problem occurred. By RF magnetron sputtering, high-quality single-phase W-$Mg_xZn_{1-x}O$ films were also synthesized with x from 0% to 36%, the band-gap energy changing from 3.25 to 4.04 eV [128]. The dark current of the MSM photodiodes with Ni/Au electrodes on such epitaxial films is less than 0.6 nA at 20 V. The cutoff wavelength shifts from 380 to 310 nm with increasing Mg content, and the rejection ratio is more than 7 × 10^2. By adopting a so-called 'homoepitaxial buffer', our group realized W − $Mg_{0.55}Zn_{0.45}O$, corresponding to a band gap of 4.55 eV [129]. The MSM photodiodes with IDT Ti/Au electrodes on this epitaxial film have a low leakage current of 3 nA at 400 V (figure 14(a)). The cutoff wavelength locates at 270 nm with a peak responsivity of 22 mA W^{-1} under 130 V (figure 14(b)), indicating a solar-blind detection capability. The UV/visible rejection ratio is more than 10^2 and response time less than 500 ns (figure 14(c)). What is more, the external quantum efficiency was found to be increased from 0.19% to 15.26% from 15 to 210 V, which indicates a large internal gain (figure 14(d)). The gain mechanism is well explained with a reduced Schottky barrier height model. Wang *et al* fabricated a fast-response Au–$Mg_{0.48}Zn_{0.62}O$–Au MSM PD on sapphire(0 0 0 1) with MOCVD. The dark current of the PD is as low as 6.5 pA at 10 V, comparable to that of the AlGaN counterpart. The responsivity is 16 mA W^{-1} at 20 V, with a cutoff wavelength at 283 nm and rejection ratio of more than 10^3. The rise and fall response times of the detector are only 10 and 150 ns, which represent the fastest response times reported with high-Mg-content W-$Mg_xZn_{1-x}O$ MSM photodiodes [130]. To gain a higher performance, some novel derivative UV photodiodes have been developed based on MSM structure. For instance, an avalanche UV photodiode with Au–MgO–$Mg_{0.44}Zn_{0.56}O$–MgO–Au symmetric structure was invented by using the MBE growth technique. The photoresponsivity is just 0.018 A W^{-1} at 2 V bias, but it increases significantly above 1000 A W^{-1} when the applied bias exceeds 31 V, where an avalanche gain of 587 was observed. The build-up of the integral gain was attributed to the impact ionization in the MgO layer at high voltage [131].

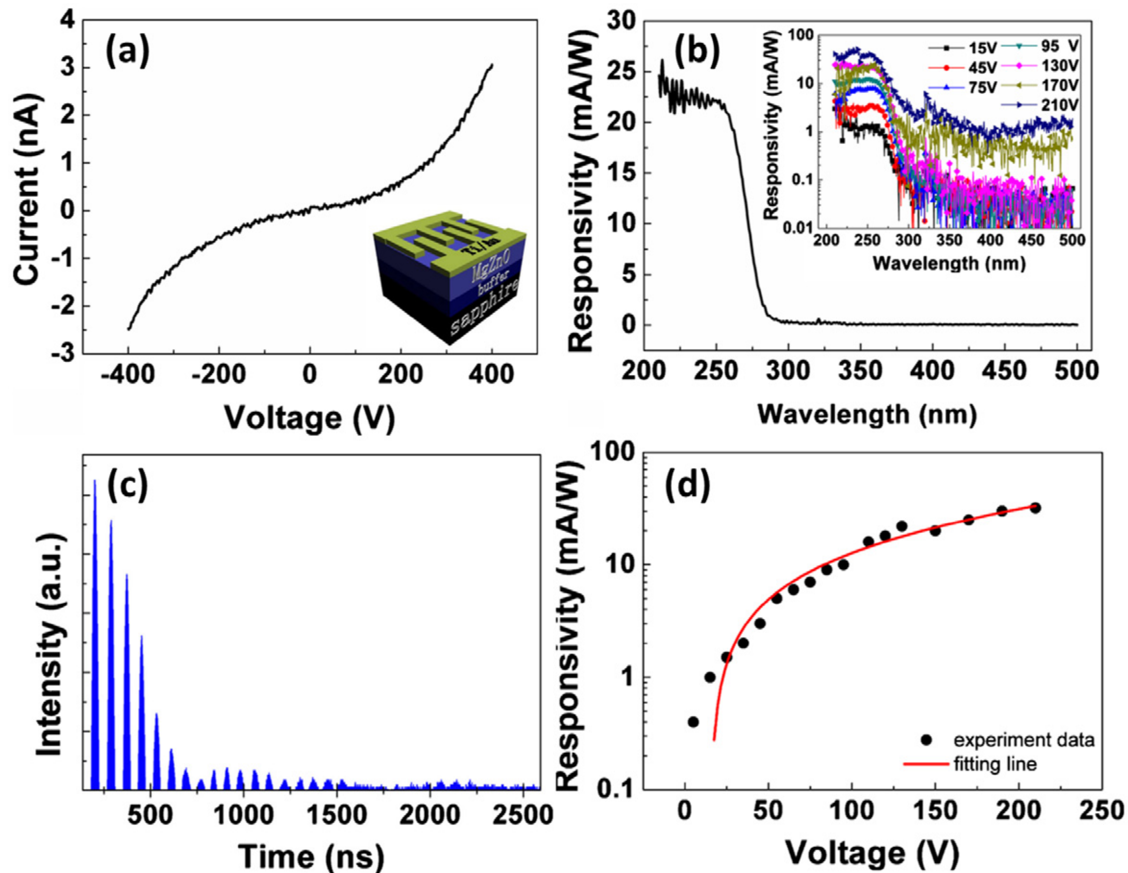

Figure 14. (*a*) Dark current of Ti/Au–$Mg_{0.55}Zn_{0.45}O$–Ti/Au MSM photodiode, (*b*) spectrum response of Ti/Au–$Mg_{0.55}Zn_{0.45}O$–Ti/Au MSM photodiode, (*c*) transient response and (*d*) peak response as a function of applied voltage. (Reprinted from [130]. Copyright 2009 Elsevier).

Although $Mg_xZn_{1-x}O$ MSM PD has been expected to integrate with well developed Si technology, high-Mg-content $W-Mg_xZn_{1-x}O$ alloy is difficult to obtain on Si substrate due to the formation of amorphous SiO_x layer at the initial growth stage of oxides and the large lattice mismatch (15.4%). In 2005, Koike *et al* first fabricated $W-Mg_xZn_{1-x}O$ MSM PDs (x: 0–43%) on Si substrate with CaF_2 buffer by MBE [132]. The cutoff wavelength shows a strong blue-shift with increasing x (figure 15). To further decrease the lattice mismatch between the epitaxial film and Si substrate, a thin BeO buffer layer was exploited for high-Mg-content $Mg_xZn_{1-x}O$ growth [133]. With plasma-assisted MBE, a $W-Mg_{0.4}Zn_{0.6}O$ epitaxial film was successfully grown on Si(1 1 1), with the band gap of 4.13 eV. An MSM photodiode was fabricated with Ti/Au electrodes on the epitaxial film. The dark current is about 0.1 nA at 3 V bias. A sharp cutoff was found at 300 nm with a rejection ratio of more than two orders of magnitude. To obtain a $Mg_xZn_{1-x}O$ UV photodiode on Si substrate with higher performance, the $Mg_xZn_{1-x}O$/Si p–n heterojunction photodiode has to be considered, which will be discussed later.

For the MSM UV photodiodes fabricated from homoepitaxial $Mg_xZn_{1-x}O$ film, a relatively thick epitaxial layer is essential to avoid the photoresponse from the ZnO substrate. With finite element modelling, intrinsic $Mg_xZn_{1-x}O$ with a thickness of 2 μm is sufficient to reduce the voltage falling on the ZnO substrate with 10 V bias [134]. To verify this, an MSM photodiode with Au IDT electrodes was fabricated on a high-quality $Mg_{0.49}Zn_{0.51}O$ film, which is 2 μm thick. Under 10 V bias, the photodiode demonstrates a low dark current of 0.36 pA, corresponding to a current density of 6.1×10^{-10} A cm^{-2}. The maximum responsivity is 304 mA W^{-1}, with a rejection ratio over 5×10^2. Another approach to prevent the photoresponse from the substrate is inserting an appropriate insulating layer between the epitaxial layer and the substrate. The insulating layer is also required to act as a good template for the epitaxial growth. Via inserting a BeO layer, a single-phase W-$Mg_{0.4}Zn_{0.6}O$ film was homoexpitaxially synthesized on ZnO substrate by MBE [135]. From the reflectance spectra characterization, the optical band gap of the film is determined as 294.5 nm (figure 16(*a*)). On this film, a photovoltaic UV-B MSM photodiode was fabricated with Ti/Au non-alloyed IDT electrodes. The cutoff wavelength locates at 290 nm, agreeing well with the reflectance spectrum peak. The maximum responsivity is approximately 20 mA W^{-1} at 260 nm, with the UV/visible rejection ratio more than two orders of magnitude (figure 16(*b*)). No photoresponse was observed from ZnO substrate, which suggests 30 nm BeO is a good electron blocking layer.

$Mg_xZn_{1-x}O$ MSM UV PDs fabricated on quartz substrates are widely reported due to cost-effective film preparation with the sputtering method [136–141]. Hullavarad *et al* compared W-$Mg_{0.15}Zn_{0.85}O$ prepared on Al_2O_3 and quartz substrates by PLD [137]. From the XRD θ–2θ scan, the film

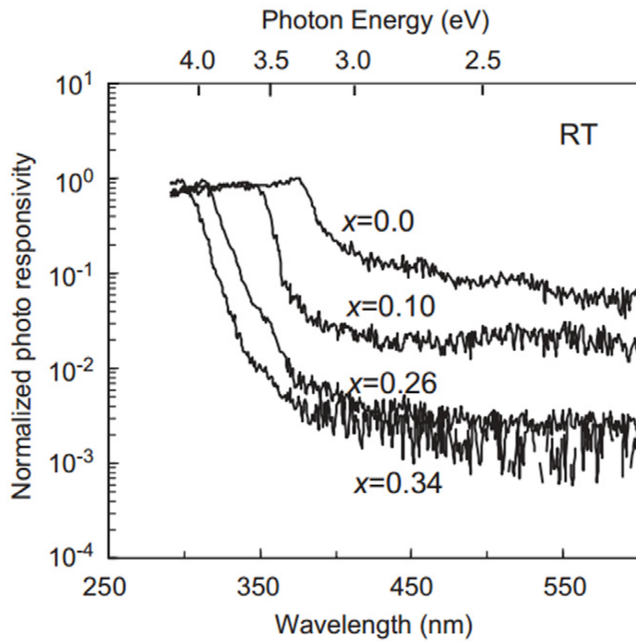

Figure 15. MSM photodiodes fabricated on MgZnO grown on Si substrate. With increasing Mg component, the detector exhibits increasing UV/visible rejection ratio and a prominent blue-shift in cutoff wavelength. (Reprinted from [132]. Copyright 2005 Elsevier).

grown on quartz shows a stronger (0 0 0 2) diffraction peak than the one on sapphire (figures 17(*a*) and (*b*)). The band gap of the thin film is 3.75 eV, determined by transmittance spectra (figure 17(*c*)). The MSM photodiodes based on such films were fabricated with Cr/Au IDT electrodes. The dark current of the device on Al_2O_3 (3×10^{-10} A) is much higher than that on quartz (1×10^{-12} A). The UV/visible rejection ratios are 10^4 and 10^3 (figure 17(*d*)), respectively. Liu *et al* reported a high-performance Au–$Mg_{0.2}Zn_{0.8}O$–Au photodiode synthesized by RF sputtering on quartz substrate [138]. The dark current of the photodiode is lower than 7 nA at 5 V bias. The peak responsivity is 0.02 A W^{-1} under 3 V, with a cutoff at 350 nm and rejection ratio of more than four orders of magnitude. The 90%–10% decay time is as fast as 170 ns. By increasing the Mg content, Zheng *et al* demonstrated a solar-blind MSM photodiode with Ti/Au electrodes on single-phase $C-Mg_{0.46}Z_{0.56}O$ (band gap 4.7 eV) film, which was fabricated on quartz with the RF sputtering method [141]. The peak responsivity is 3.4 A W^{-1} at 280 nm under 10 V, with a large rejection ratio of more than 10^3 and fast response speed of less than 482 μs. A large internal gain of 148 is found when the applied bias is 70 V, which is attributed to acceptor-like deep-level defects located at E_v + 282 meV according to the deep-level transient spectrum (DLTS) characterization.

Deep-UV MSM photodiodes based on $C-Mg_xZn_{1-x}O$ were also explored, as it is a complementary material to $W-Mg_xZn_{1-x}O$. Jiang *et al* reported an MSM UV photodiode based on $C-Mg_{0.7}Zn_{0.3}O$ fabricated by RF sputtering on quartz substrate in 2009 [142]. The cutoff wavelength is 230 nm, in the solar-blind region. By accommodating the mole ratio of Zn and Mg precursors, single-phase $C-Mg_xZn_{1-x}O$ thin films with x from 70% down to 50% were

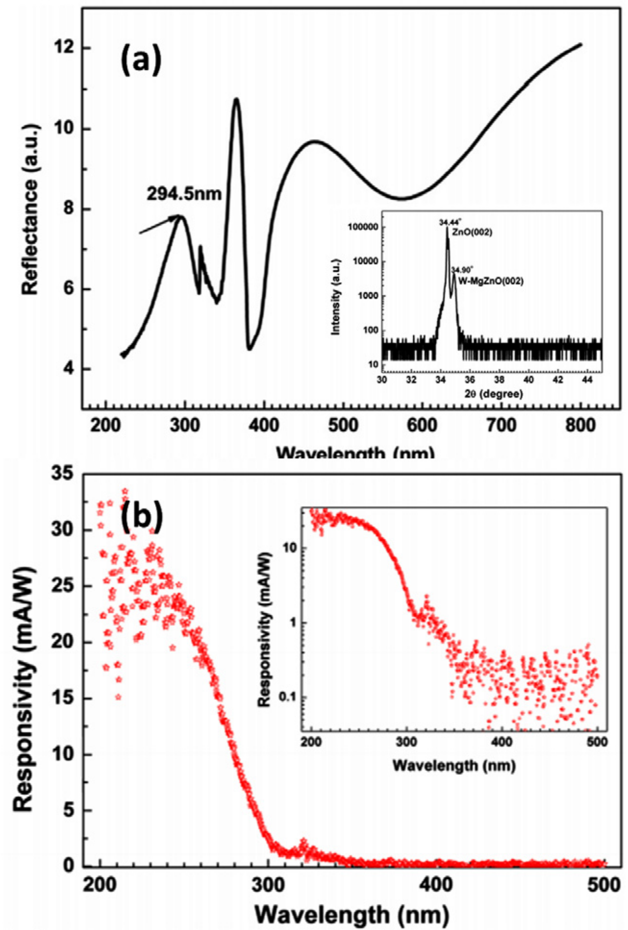

Figure 16. (*a*) Reflectance spectrum of W-$Mg_{0.4}Zn_{0.6}O$ measured at room temperature. Inset showing the XRD θ–2θ scan; only a single peak was observed. (*b*) Photoresponse spectrum at 0 V bias; the inset shows the result in a logarithmic scale. (Reprinted from [135]. Copyright 2013 Elsevier).

realized by the MOCVD growth method [143]. From the transmittance spectra, the absorption edge shifts from 220 to 260 nm with decreasing Mg content. Based on such films, MSM photodiodes were fabricated with 2 μm gap Au IDT electrodes. The cutoff wavelength varies from 225 to 287 nm with decreasing Mg content. For representation, the peak responsivity of the detector on $Mg_{0.52}Zn_{0.48}O$ is about 0.1 mA W^{-1} at 250 nm, with a cutoff wavelength of 273 nm and rejection ratio of more than 10^4. The peak responsivity shows a linear relationship with applied voltage from 0 to 30 V, indicating no carrier mobility saturation and sweep-out effect. Han *et al* noticed that surface roughness of $C-Mg_xZn_{1-x}O$ can be greatly improved by using a MgO buffer layer during MOCVD growth, which is beneficial for the subsequent performance of the MSM photodiode [144]. In the meantime, the sub-band gap light response can be efficiently suppressed.

4. P–n junction photodiodes

The p–n junction photodiode is the most important semiconductor PD, as the basic carrier transport theory is built on it. It is formed due to the electron–hole diffusion and

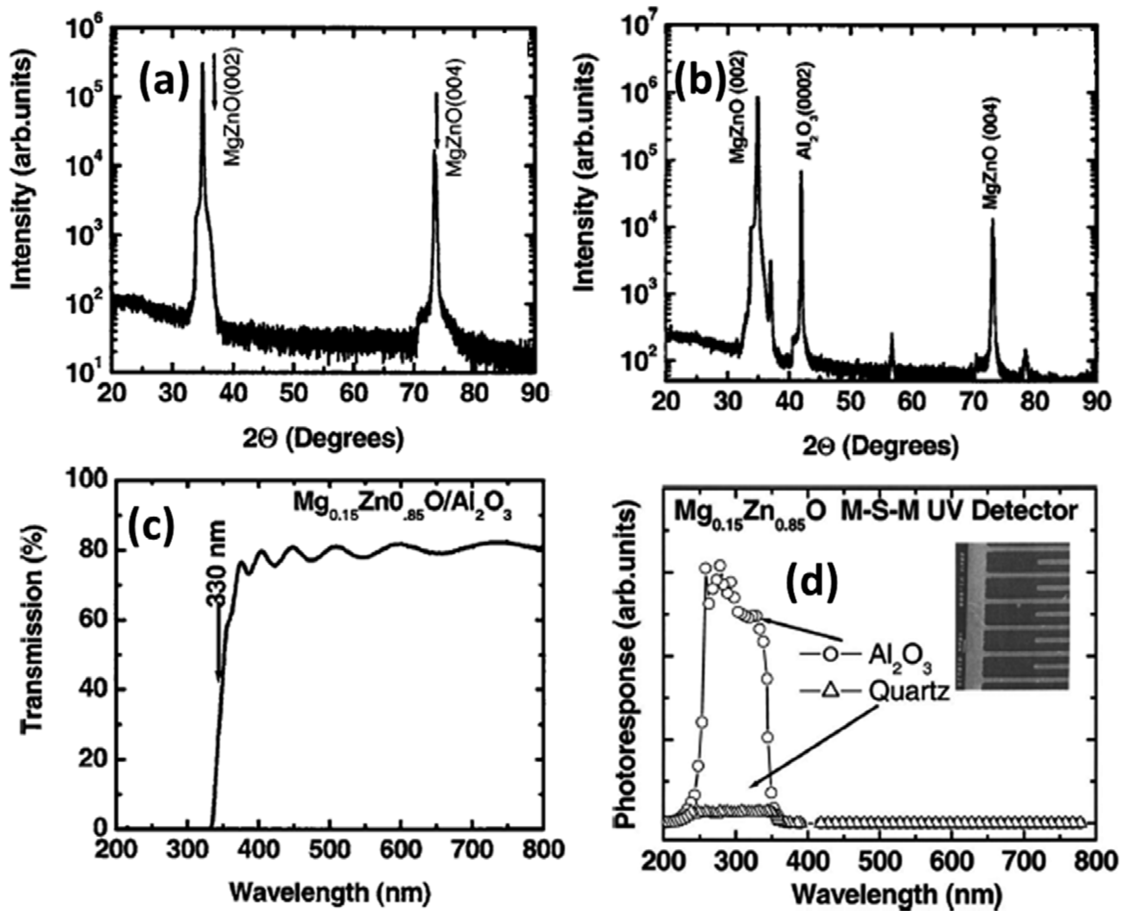

Figure 17. X-ray diffraction pattern of $Mg_{0.15}Zn_{0.85}O$ on quartz (*a*) and Al_2O_3 substrate (*b*). (*c*) UV/visible transmission spectrum of $Mg_{0.15}Zn_{0.85}O$ on Al_2O_3 showing a strong absorption at 330 nm. (*d*) Photoresponse spectra of $Mg_{0.15}Zn_{0.85}O$ on quartz and Al_2O_3 substrates, respectively. The inset shows a microscope image of the IDT electrode configuration of the MSM device. (Reprinted from [137]. Copyright 2005 AIP Publishing LLC).

recombination between a p-type doped and the adjacent n-type doped semiconductor. Due to the depletion of carriers, a built-in electric field directed from the n-type to the p-type semiconductor will be created in the space charged region. The distribution of built-in electric field and energy band diagram are schematically shown in figure 18(*a*). When the photodiode is under illumination, electron–hole pairs generated in the space charge region will be separated and collected by the electrodes, producing photoresponse current (figure 18(*b*)).

Based on diffusion theory, Shockley proposed the famous carrier transport equation,

$$J_0 = J_{0\mathrm{pn}}\left[\exp\left(qV/nkT\right)\right] \tag{4.1}$$

where q, V, n, k and T are unit electron charge, applied bias, ideality factor, Boltzmann constant and absolute temperature, respectively. $J_{0\mathrm{pn}}$ is the reverse saturated current, which is

$$J_{0\mathrm{pn}} = qD_\mathrm{p}p_{\mathrm{n}0}/L_\mathrm{p} + qD_\mathrm{n}p_{\mathrm{p}0}/L_\mathrm{n} \tag{4.2}$$

where D_p and D_n are the doping intensities, $p_{\mathrm{n}0}$ and $n_{\mathrm{p}0}$ are the minority carrier intensities, $L_\mathrm{p}\left(L_\mathrm{p} = \sqrt{(D_\mathrm{p}\tau_\mathrm{p})}\right)$ and $L_\mathrm{n}\left(L_\mathrm{n} = \sqrt{(D_\mathrm{n}\tau_\mathrm{n})}\right)$ are the carrier diffusion lengths, and τ_n and τ_p are the minority carrier lifetimes. Comparing equation (4.1) to (3.2), one can see the basic transport equations are in exactly the same format for both Schottky and p–n junction diodes. However, in contrast to the Schottky diode, the conductive properties of the p–n diode are dominated by minority carriers. The current will be changed severely even there is just a tiny change in the minority carrier density. From this point of view, the p–n junction is more sensitive to the incident light than the Schottky photodiodes, but the response speed is slower, due to the restricted carrier diffusion speed.

4.1. ZnO p–n junction photodiodes

4.1.1. ZnO homojunction photodiodes. P-type ZnO is essential for p–n homojunction diodes, which are not only meaningful for PDs, but also the key element for ZnO-based light emitting devices [145, 146]. As a result of the existence of intrinsic deep-level defects and lack of appropriate shallow acceptor dopants, reliable p-type conductive ZnO film is difficult to acquire [147, 148]. Thus only a limited number of reports on ZnO p–n homojunction UV photodiodes can be found. The typical dopants used for these p–n homojunction photodiodes include As, Sb and $LiNO_3$ [149–151].

The earliest prototype ZnO p–n homojunction photodiode was reported by Moon *et al* [152]. They first grew an

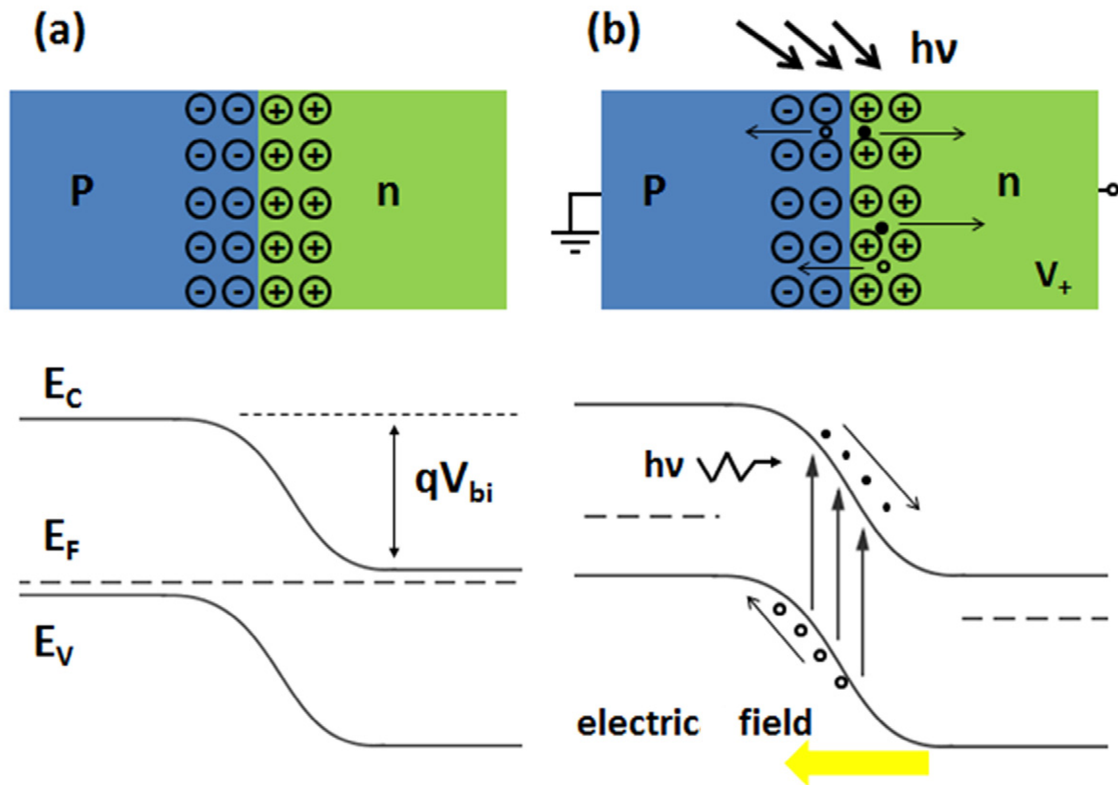

Figure 18. Diagram of a p–n junction under (*a*) equilibrium and (*b*) illumination conditions.

unintentionally n-doped ZnO layer on GaAs substrate by RF sputtering, and then carried out a diffusion process at 600 °C. P-type ZnO : As was obtained as As atoms diffused from the substrate into ZnO film. Finally, the n-type ZnO : Al was deposited on the top to form a p-ZnO : As/n-ZnO:Al photodiode. The photodiode shows a noticeable current difference before and after 365 nm UV illumination, while it is insensitive to visible light. In the same period, Ryu *et al* reported a high-performance p-ZnO : As/n-ZnO diode by hybrid deposition [149]. The dark leakage current is lower than 10^{-6} A cm^{-2}, and the photo-to-dark current ratio at zero bias is as high as 20 (figure 19(*a*)). From the photoresponse spectra, a sharp near band edge response peak at 380 nm and a deep-level defect related response shoulder at 460 nm were observed (figure 19(*b*)). Apart from this, homojunction UV photodiodes based on Sb doped p-type ZnO grown by MBE were also studied [150, 153–155]. Their steady state and transient photoresponse properties show similar behaviour to the one based on As doped p-type ZnO. It is worth highlighting that the p-type layer is likely fully depleted due to the low p-type doping efficiency. Such degradation of the p-layer into an i-layer will cause a reduction of quantum efficiency or raise an unwanted photoresponse from the extension of the depletion region into other layers [153, 154]. To avoid this situation, a thicker p-type layer or p–i–n structure has been exploited [150, 151, 155]. With a newly promoted growth technology, a method of vapour cooling condensation was used for p-type ZnO preparation. With this technique, Lin and Lee presented a p–i–n (p-ZnO : $LiNO_3$–i-ZnO–n-ZnO:In) photodiode on sapphire substrate [151]. The detector has a high responsivity of 0.052 A W^{-1} and rejection ratio of 2.82×10^3 at −1 V. The detectivity at −1 V is as high as 5.53×10^{11} cm Hz$^{1/2}$ W^{-1}, which suggests the device can work with a low noise level. From the noise power density measurement, low-frequency noise is dominated by flicker noise.

4.1.2. ZnO heterojunction photodiodes. To circumvent the obstacles of ZnO p-type doping issues, heterojunction p–n photodiodes have been studied intensively. In order to match the energy band structure of ZnO, the heterojunction photodiodes are frequently constructed on p-type WBG semiconductors, such as NiO, GaN, SiC and diamond. These substrates are transparent to visible light because of their large band-gap energy. Among them, NiO shares some similar merits with ZnO, such as low cost and easy fabrication, and they are both oxide semiconductors. Therefore, UV photodiodes based on ZnO/NiO heterojunctions attracted the attention of many groups. In 2003, Ohta *et al* reported a high-performance p-NiO : Li/n-ZnO photodiode fabricated by PLD [156, 157]. The detector has a low dark current, with an ideality factor and turn-on voltage of 2 and 1 V (figure 20(*a*)), respectively. The photoresponsivity is 0.3 A W^{-1} at 360 nm (figure 20(*b*)), comparable to the value of commercial GaN UV detectors. With e-beam deposition, a comparative study on the properties of p-NiO–i-ZnO–n-ITO (p–i–n) and n-ITO–i-ZnO–p-NiO (n–i–p) photodiodes has been carried out [158]. The maximum quantum efficiency of p–i–n photodiodes (18%) is much higher than that of n–i–p diodes (6%), due to its lower optical loss in the top ITO contact. P-NiO/n-ZnO heterojunction UV photodiodes fabricated by the

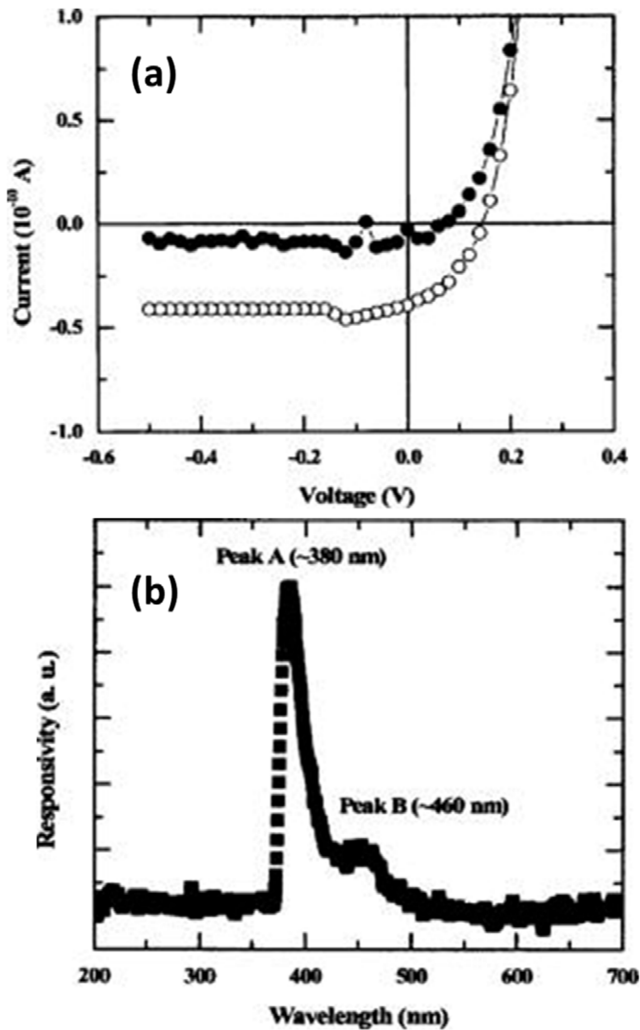

Figure 19. (a) I–V characterization of p-ZnO : As/n-ZnO UV photodiode in the dark and under UV illumination, and (b) spectrum response of p-ZnO : As/n-ZnO UV photodiode. (Reprinted from [149]. Copyright 2005 AIP Publishing LLC).

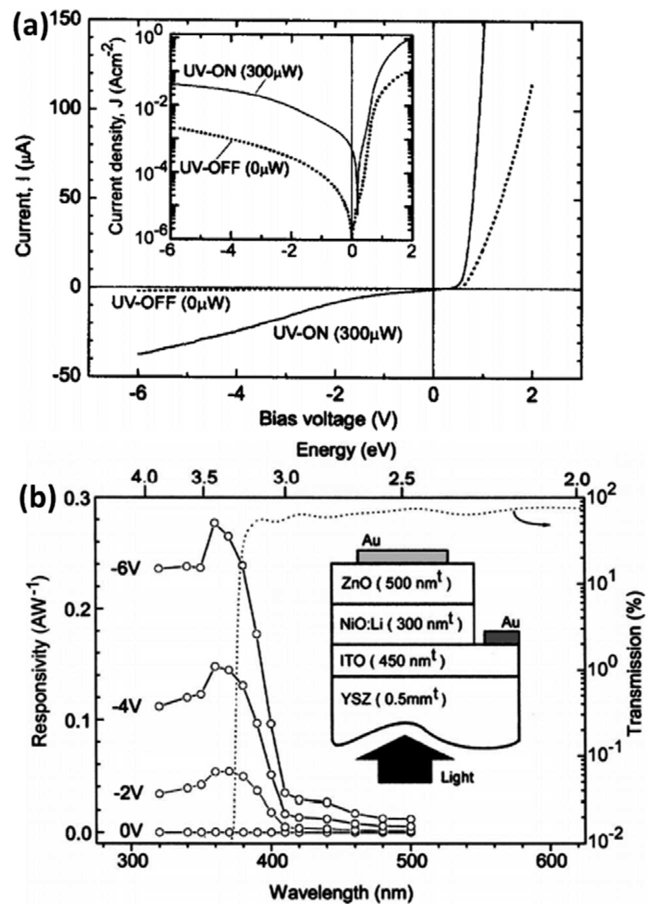

Figure 20. (a) I–V characterization of a p-NiO : Li/n-ZnO UV photodiode fabricated by PLD and (b) spectrum response of the p-NiO : Li/n-ZnO UV photodiode. (Reprinted from [156]. Copyright 2003 AIP Publishing LLC).

sputtering method also have been studied [159, 160]. The UV detectors exhibit either fast response or high photoresponsivity. Recently, Park *et al* demonstrated a p-NiO/n-ZnO photodiode fabricated by the low cost sol–gel spin coating method. The photodiode shows a good rectification ratio of 50 at ± 5 V, indicating a relatively low interface disorder. At -5 V, a peak photoresponse of 21.8 A W^{-1} was observed, with a UV/visible rejection ratio of 1.6×10^3 [161].

Diamond substrate is considered as another potential substrate suitable for ZnO-based heterostructure photodiodes, which might be sufficient for special applications [162]. Huang *et al* demonstrated a ZnO/diamond UV photodiode configured with highly c-plane oriented ZnO grown on free-standing diamond by hot filament chemical vapour deposition (HFCVD) [163]. The photodiode displays a high rectification ratio of 8×10^4 at $\pm$ 3.5 V and a low turn-on voltage of 1.6 V. The peak responsivity locating at 370 nm exceeds 0.2 A W^{-1} at reversed 3 V bias, comparable to that of commercial GaN UV photodiodes.

6 H-SiC has a small lattice mismatch with ZnO (4%), ideal for ZnO heteroepitaxial growth. However, it is difficult to get rid of substrate response as a result of its narrower band gap of 2.9 eV compared with the 3.34 eV of ZnO. Alivov *et al* reported a heterojunction n-ZnO/p-6H-SiC UV photodiode by MBE [164]. The I–V curve shows a good rectifying behaviour with low leakage current $<10^{-7}$ A at 20 V and a high breakdown voltage >20 V. From the photoresponse spectra, the responsivity is as high as 0.045 A W^{-1} at reversed 7.5 V, with a shoulder response at 3.05 V from the substrate.

Compared with NiO, diamond and SiC, GaN has the same lattice structure as ZnO, with a relatively low mismatch of 1.8%. What is more, p-type GaN is readily available. Hence, it is the most promising for ZnO heterojunction preparation with low interface defects [165]. A band-pass n-ZnO/p-GaN photodiode has been invented with MBE growth techniques [166]. The I–V characterization reveals a clear rectifying behaviour with turn-on voltage at 4.6 V. The GaN layer acts as not only a hole pool but also a 'filter'. Under back-illumination, the photoresponse spectrum shows a narrow band centred at 374 nm with a full-width at half-maximum value of only 17 nm, revealing a highly selective response property. Al-Zouhbi *et al* developed a ZnO/GaN heterojunction photodiode by the spray pyrolysis method [167]. A prominent rectification character was observed from I–V measurement, with turn-on voltage of 1 V and ideality factor of 13.35. The large n value can be

explained in terms of the interface states and series resistance. The decay time is as long as 30 s, which is related to the interface states, corresponding to the large n value.

Si substrates are widely used for ZnO heterojunction photodiodes in spite of the large lattice mismatch, thanks to the mature Si based microelectronic technology. Because the long-wavelength photoresponse from Si substrate is difficult to suppress, ZnO/Si photodiodes usually detect both UV light and visible light simultaneously. In 2003, Jeong *et al* reported their investigation on an n-ZnO/p-Si photodiode fabricated by RF sputtering [168]. The diodes exhibit strong responsivities of 0.5 and 0.3 A W^{-1} for UV (∼310 nm) and red (∼650 nm) photons under −30 V, respectively. The UV/visible detection principle was explained with its energy band structure. Under reverse bias, the photogenerated holes in the ZnO layer can transport through the valence band offsets to form a UV photoresponse, whilst photogenerated electrons in the Si will be transported to the ZnO side to raise a visible light response. In a similar structure of Ni/n-ZnO/p-Si, Kosyachenko *et al* observed a large internal gain [169]. Under 5 V, the responsivities at $\lambda = 390$ nm and 850 nm are 210 A W^{-1} and 110 A W^{-1}, corresponding to large quantum efficiencies of 655 and 165, respectively. The large internal gain lies in the Schottky contact between Ni and ZnO, which acts like an emitter junction of a bipolar transistor. Under UV illumination, the photogenerated holes from the emitter will be swept through the base (ZnO) into the collector (p-Si). Therefore, an amplified photocurrent will be obtained.

To optimize the device performance, several approaches have been attempted, including device isolation, surface coating and doping. Park *et al* obtained isolated ZnO/Si heterojunction photodiodes by Si^+ ion implantation [170]. The maximum quantum efficiency is 70% (0.35 A W^{-1}) under 5 V at 650 nm, which decreases to 10% at 420 nm. The efficiency drop in the UV range was attributed to the light absorption before reaching the Si optically active area. Chen *et al* reported a ZnO/Si photodiode coated with silica nanoparticles [171]. As the transmittance is improved by the coating layer, the average photoresponsivity was promoted by 17.6% compared with the uncoated value. Moreover, due to Bragg diffraction, the acceptance angle was markedly increased. Gupta *et al* studied the effect of doping on the photodiode performance [172]. By the sol–gel method, they fabricated a series of n-ZnO : Al/p-Si with Al contents of 0%, 0.6%, 0.8% and 1%. The highest photoresponsivity of 0.22 A W^{-1} at reverse 5 V was found with the doping concentration of 0.8%, compared to 0.01 A W^{-1} for the undoped photodiode.

Intending to get rid of the visible light response from Si substrate and achieve net UV signal detection, a new device configuration has been designed. We have proposed a kind of n-ZnO–i-MgO–p-Si (p–i–n) photodiode fabricated by MBE [173]. The I–V curve exhibits a distinct rectifying character, with rectification ratio of 104 at ±2 V and low leakage current of 1 nA at −2 V. From the photoresponse spectra, a steep cutoff edge was observed at 378 nm, corresponding to the near band edge absorption. No visible light response was observed within the whole spectra. The energy band diagram was used to illustrate the principle of the photodiode. Under the equilibrium state, a high electron barrier of 3.2 eV forms between Si and MgO, and a relatively low hole barrier of 0.83 eV occurs at the MgO/ZnO interface (figure 21(*a*)). When the device is under illumination at a reverse bias, UV light generated holes in the ZnO layer can be transported over the barrier and reach the Si side to build up photocurrent. However, the visible light generated electrons are effectively blocked by the potential barrier and recombined with holes, without generating photocurrent (figure 21(*b*)). A similar device structure has also been fabricated with $LaAlO_3$ or SiO_2 as the insulating layer [174, 175].

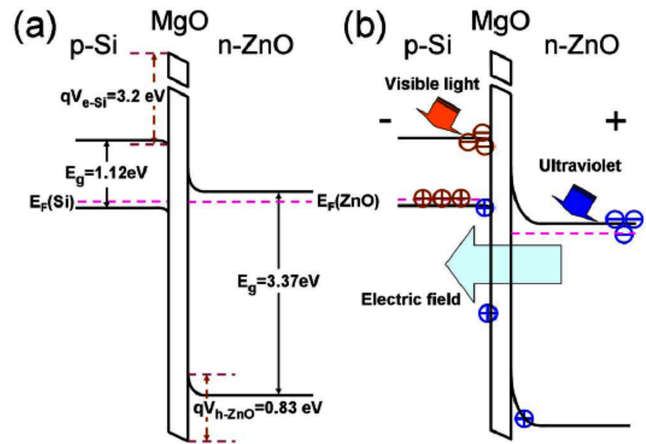

Figure 21. The energy band diagram of an n-ZnO/p-Si UV photodiode under (*a*) equilibrium conditions and (*b*) illumination at a reverse bias. (Reprinted from [173]. Copyright 2009 AIP Publishing LLC).

4.2. MgZnO p–n junction photodiodes

4.2.1. MgZnO homojunction photodiodes. For the same reason as for ZnO, reliable p-type $Mg_xZn_{1-x}O$ is extraordinarily difficult to achieve. Therefore, only a few groups have reported homojunction photodiodes based on $Mg_xZn_{1-x}O$. In 2007, Liu *et al* demonstrated a p–n homojunction photodiode with N-doped $Mg_{0.24}Zn_{0.76}O$ by MBE [176]. The p-type film possesses a high orientation, a hole concentration of 1×10^{16} cm^{-3} and a transmittance of more than 75% in the visible light region. From the I–V characterization, a weak rectification ratio was observed, with a turn-on voltage at 2 V. The weak rectifying behaviour is attributed to the low quality of the p-$Mg_{0.24}Zn_{0.76}O$ film. From the spectrum response, the cutoff wavelength occurs at 345 nm, in accordance with the band gap of $Mg_{0.24}Zn_{0.76}O$. The peak responsivity increases linearly from 3.7×10^{-6} to 4×10^{-4} A W^{-1} when the reverse voltage increases from 0 to 9 V, with UV/visible rejection ratio more than 10^4. The PD has a fast response time of less than 10 ns in rise and 150 ns in fall. In 2009, Shukla developed a homojunction photodiode based on gallium doped n-$Mg_xZn_{1-x}O$ and phosphor doped p-$Mg_xZn_{1-x}O$ by PLD, with x from 0% to 34% [177]. The carrier concentration and mobility of the p-type film are 10^{16} cm^{-3} and 1 cm^2 V s^{-1}, respectively. The dark reverse current is smaller than 2 nA under 40 V. From the spectrum response, the cutoff wavelength of the

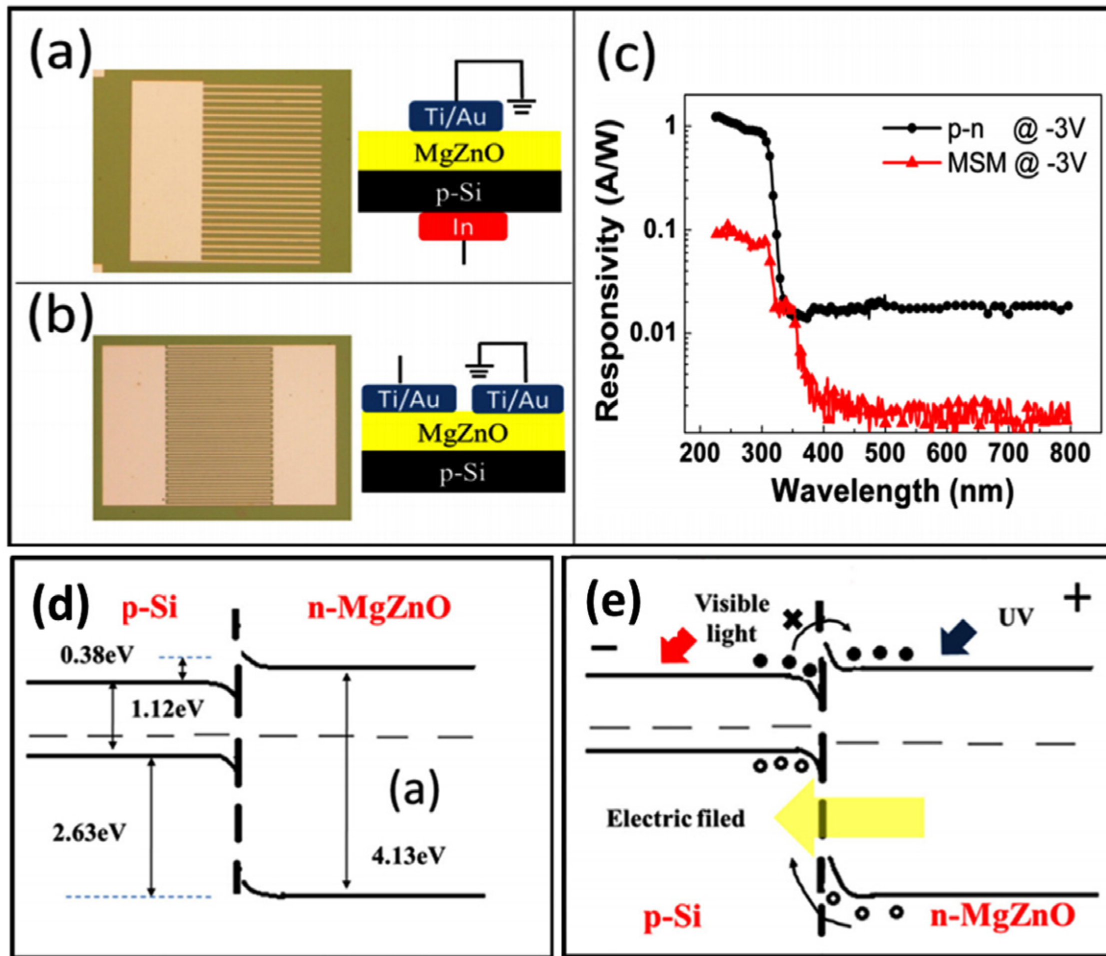

Figure 22. (*a*) Schematic diagram of an n-MgZnO/p-Si UV photodiode grown by MBE, (*b*) diagram of a TiAu/MgZnO MSM UV photodiode grown by MBE, (*c*) comparison of the spectrum response of the photodiodes, (*d*) energy band diagram of n-MgZnO/p-Si UV photodiode under equilibrium conditions and (*e*) energy band diagram of n-MgZnO/p-Si UV photodiode under illumination at reverse bias. (Reprinted from [133]. Copyright 2011 AIP Publishing LLC).

detectors shows a clear blue-shift from 380 to 284 nm. P–n junction photodiodes configured with p-$Mg_xZn_{1-x}O$/ZnO were also reported [178, 179]. The cutoff wavelength of such photodiodes is determined by the ZnO layer, as the band gap of $Mg_xZn_{1-x}O$ is larger than that of ZnO. It should be noticed that the p-type $Mg_xZn_{1-x}O$ has a carrier density of 10^{16} cm^{-3}, two orders of magnitude lower than that of n type for the same reason as p-type ZnO doping [176, 177, 179]. Special consideration should be given to the depletion of the p-type layer for such devices.

4.2.2. MgZnO heterojunction photodiodes. The heterojunction photodiode is a possible option to avoid p-type doping problems, although it is difficult to get high-quality single-phase $Mg_xZn_{1-x}O$ films without phase segregation by heteroepitaxial growth. By using a low-temperature oxidized BeO buffer layer, our group solved this problem and successfully synthesized high-quality single-phase high-Mg-content W − $Mg_xZn_{1-x}O$ (x = 0.4) film on Si substrate [133, 180]. Further, the epitaxial film was processed into n-MgZnO/p-Si heterojunction and MSM photodiodes (as shown in figures 22(*a*) and (*b*)), and their performances were comparatively studied. It is found the leakage current at reverse 3 V is lower than 1 nA for both of the photodiodes. From the spectrum response characterization (figure 22(*c*)), the photoresponsivity of the p–n heterojunction photodiode (1 A W^{-1}) is one order of magnitude larger than that of its MSM counterpart (0.1 A W^{-1}). No photoresponse from the Si substrate was observed. The working principle of the heterojunction photodiode is illustrated from the energy band diagram shown in figure 22(*d*). The conduction band and valence band expansion ratio is 9 : 1 when MgZnO alloy is formed by substituting Zn atoms with Mg [181]. Therefore, a type-I heterojunction will form between high-Mg-content $Mg_xZn_{1-x}O$ films and Si, differing from the type-II heterojunction at the ZnO/Si interface. When the diode is under illumination at a reverse bias (figure 22(*e*)), UV generated holes in the $Mg_xZn_{1-x}O$ layer can be transported to the Si over the valence band offset. However, the visible light generated electrons in the Si substrate will be blocked by the conduction band offset between $Mg_xZn_{1-x}O$ and Si. As a result, only UV response was observed. By accommodating the Mg flux elaborately during growth, a higher Mg content single-phase W-$Mg_xZn_{1-x}O$ film was realized on Si [182].

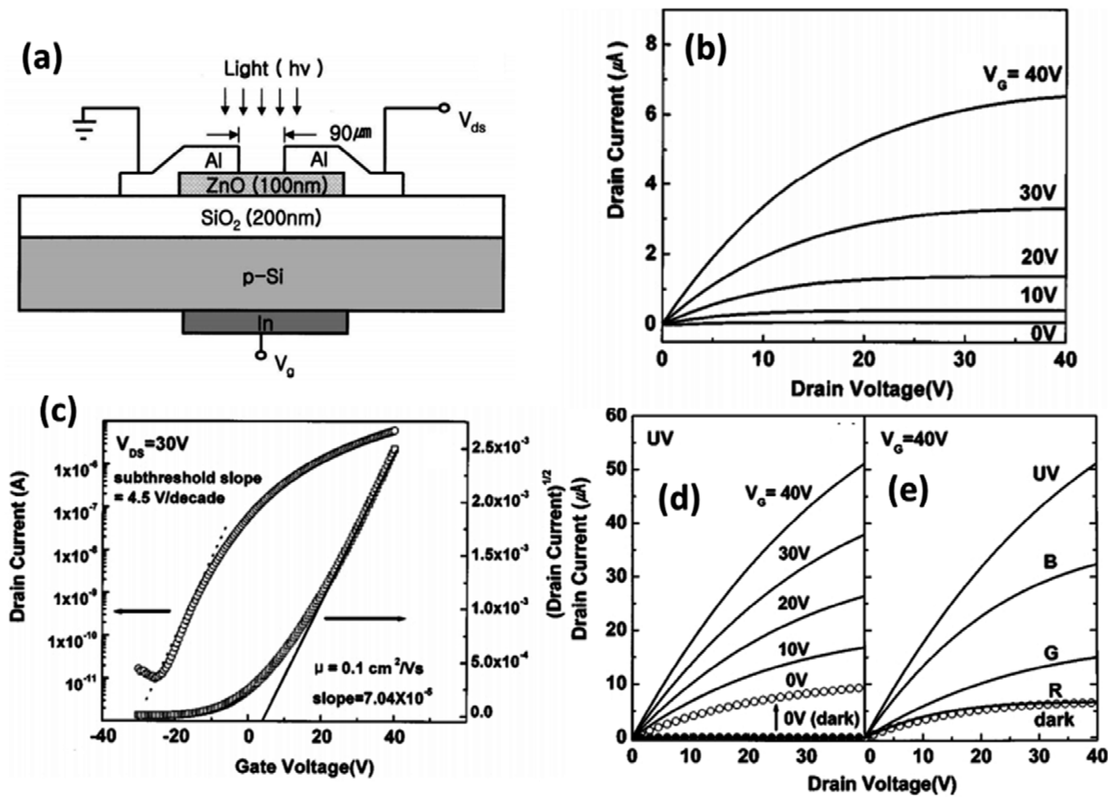

Figure 23. (*a*) Device structure of a ZnO phototransistor, (*b*) $I_D - V_D$ characterization of the photodiode in the dark, (*c*) the $I_D - V_g$ characterization of the photodiode, (*d*) $I_D - V_D$ characterization of the photodiode under UV illumination and (*e*) spectrum response of the phototransistor under R, G, B and UV illumination. (Reprinted from [185]. Copyright 2004 Elsevier).

The p–n junction photodiode fabricated on this film shows a low leakage current of 2 nA at reverse 3 V and a sharp cutoff at 280 nm, which is right in the solar-blind region. This is the first report of a $Mg_xZn_{1-x}O$/Si solar-blind UV detector to our knowledge. Based on these achievements, we fabricated a UV photodiode based on a multi-layer $Mg_xZn_{1-x}O$ [183]. Under reverse bias, the response spectrum shows a responsivity of 6 mA W^{-1} at 301 nm, whilst a cutoff was found at 280 nm with a responsivity of 13 mA W^{-1} at forward bias. Therefore, the detector is capable of detecting both solar-blind and visible-blind UV light by controlling the polarity of the applied bias. The working mechanism is well interpreted with an asymmetric quantum well scattering process.

5. ZnO-based phototransistor

Thin-film transistors (TFTs) based on ZnO have attracted much attention recently on account of their high field mobility (μ_E), high transparency to visible light, low price of the raw material and simple fabrication process. A phototransistor is identical to a TFT in device structure, with the channel layer acting as an optically active area. Compared to the traditional UV PDs, the phototransistor has a gigantic responsivity as the drain current (I_D) can be amplified by controlling the gate voltage (V_g). The response time is dominated by the on/off time of the phototransistor, which can be used to erase the persistent photocurrent (PPC) effect. Such a functional hybrid optoelectronic device is a new member of the high-performance UV photodiodes based on ZnO materials.

Bae *et al* first demonstrated a UV sensitive ZnO TFT on Si substrate by RF sputtering, as shown in figure 23(*a*) [184, 185]. The drain current–drain voltage ($I_D - V_D$) and drain current–gate voltage ($I_D - V_G$) curves are shown in figures 23(*b*) and (*c*), from which the mobility and on/off ratio are determined as 0.1 $cm^2 V^{-1} s^{-1}$ and $\sim 10^6$, respectively. The dark saturation current is about 6 μA under 40 V gate voltage. Figure 23(*d*) shows the $I_D - V_D$ relationship under 340 nm UV light illumination. It can be seen that the saturation current is tremendously enhanced compared to the dark current. An increase from 6 to 50 μA was found under 40 V gate voltage. The spectral photoelectric response was obtained under illumination of monochromatic photons with UV (340 nm), blue (450 nm), green (540 nm) and red (650 nm) under a gate bias of 40 V (figure 23(*e*)). The highest photocurrent was found at 340 nm, corresponding to the near band edge recombination. However, visible response was also found when the photon energy exceeded 2.3 eV, which is ascribed to the photoresponse from the mid-band-gap states.

Reyes *et al* developed a phototransistor with an oxygen plasma treated ZnO channel [186]. The device operates in an enhancement mode with a high field effect mobility μ_{FE} of 32.4 $cm^2 V^{-1} s^{-1}$ and a high on–off ratio of 10^{10}. The dark current is only 5×10^{-14} A under a gate bias of −10 V. From the spectrum response, the cutoff wavelength locates at 376 nm, with a UV/dark rejection ratio of more than 10^4.

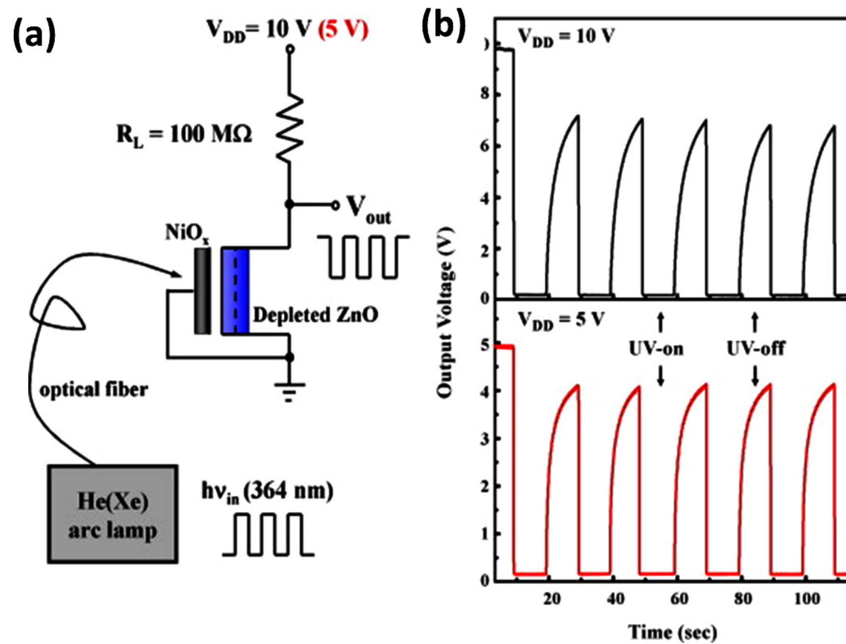

Figure 24. (*a*) An optical converter based on a ZnO phototransistor and (*b*) the output signals of the inverter at 10 V (top panel) and 5 V (bottom panel). (Reprinted from [187]. Copyright 2008 Elsevier).

Most importantly, the PPC effect is effectively suppressed under positive gate bias. From the transient photoresponse measurement, the switch-off time is only 5 ms under positive gate bias, compared to 29 ms under negative gate bias. The slowing down of the recombination process under reverse gate bias is due to the separation of UV generated electron–hole pairs in the large depletion region. On the other hand, positive gate bias provides a conduction path for the separated carriers to drain out of the channel.

For the practical applications of ZnO phototransistors, Lee *et al* demonstrated an optical inverter [187, 188]. The inverter consists of a ZnO phototransistor and a load resistor, which facilitates measurement of the dynamic UV response signal during the inverting action. The basic concept of the optical inverter is based on the electrical inverter composed of a transistor and a load resistor, except that the input gate voltage pulse is replaced by a UV pulse for optical gating (figure 24(*a*)). The output signals of the inverter are shown in figure 24(*b*) under source biases of 10 and 5 V. Obviously, when the UV is 'off', the output voltage is 'on', and vice versa. However, the output voltage is lower than the input one, and the response time after UV off is slow. This is attributed to the aforementioned mid-gap state response. In addition, a real-time UV PD of light erasable memory based on an InGaZnO (a kind of quaternary alloy of ZnO) phototransistor was also proposed [189]. The writing process is performed with a forward gate bias to switch the memory from a high-resistance to a low-resistance state, whilst the erasing process is conducted by a reverse biased gate bias combined with UV illumination to switch the device from a low-resistance to a high-resistance state. It is found that the device conductance produced by either writing or erasing can be well maintained for 10 000 s, with an on/off ratio of 10^4. Therefore, ZnO UV phototransistors can work as functional PDs, which could be used for future optoelectronic logic circuits.

6. Summary

We have reviewed the recent development of ZnO and $Mg_xZn_{1-x}O$ based UV PDs. In the past few years, ZnO-based UV detectors have been fabricated with planar structure or vertical structures on various substrates. The detection properties of some devices are actually much better than current commercial UV detectors. With band-gap engineering techniques, high-performance deep-UV PDs with different bandwidths based on $Mg_xZn_{1-x}O$ have been achieved. Multi-waveband and wavelength-selective UV detection on a monolithic chip were realized with novel device structures. What is more, a hybrid device structure such as a phototransistor provides new approaches to construct high-quality UV PDs which could be applicable for different optoelectronic circuits. For the forthcoming commercial ZnO-based UV PDs, the bottleneck still lies in the deep-level states of the films with a cost-effective growth approach, such as sputtering, CVD, sol–gel and spray pyrolysis, which we believe will be solved in the near future.

Acknowledgments

This work was supported by the Ministry of Science and Technology of China (grant nos 2011CB302002, 2011CB302006), the National Science Foundation of China (grant nos 11174348, 51272280, 11274366, 61204067, 61306011) and the Chinese Academy of Sciences.

References

[1] Muñoz E, Monroy E, Pau J L, Calle F, Omnès F and Gibart P 2001 *J. Phys.: Condens. Matter* **13** 7115
[2] Lin H W, Ku S Y, Su H C, Huang C W, Lin Y T, Wong K T and Wu C C 2005 *Adv. Mater.* **17** 2489–93
[3] Xu Z and Sadler B M 2008 *IEEE Commun. Mag.* **46** 67–73
[4] Monroy E, Omnès F and Calle F 2003 *Semicond. Sci. Technol.* **18** R33
[5] Razeghi M and Rogalski A 1996 *J. Appl. Phys.* **79** 7433–73
[6] Morkoç H, Carlob A D and Cingolania R 2002 *Solid-State Electron.* **46** 157–202
[7] Mohammad S N and Morkoç H 1996 *Prog. Quantum Electron.* **20** 361–525
[8] Parish G, Keller S, Kozodoy P, Ibbetson J P, Marchand H, Fini P T, Fleischer S B, DenBaars S P, Mishra U K and Tarsa E J 1999 *Appl. Phys. Lett.* **75** 247
[9] Tsukazaki A, Akasaka S, Nakahara K, Ohno Y, Ohno H, Maryenko D, Ohtomo A and Kawasaki M 2010 *Nature Mater.* **9** 889–93
[10] Auret F D, Goodman S A, Hayes M, Legodi M J, van Laarhoven H A and Look D C 2001 *Appl. Phys. Lett.* **79** 3074
[11] Yamada H, Chayahara A, Mokuno Y, Umezawa H, Shikata S and Fujimori N 2010 *Appl. Phys. Express* **3** 051301
[12] Aida H, Nishiguchi K, Takeda H, Aota N, Sunakawa K and Yanuchi Y 2008 *Japan. J. Appl. Phys.* **47** 8506–9
[13] Oshima T, Okuno T, Arai N, Suzuki N, Hino H and Fujita S 2009 *Japan. J. Appl. Phys.* **48** 011605
[14] Koide Y, Liao M Y, Alvarez J, Imura M, Sueishi K and Yoshifusa F 2009 *Nano–Micro Lett.* **1** 30–3
[15] Hsu J W P, Tallant D R, Simpson R L, Missert N A and Copeland R G 2006 *Appl. Phys. Lett.* **88** 252103
[16] Boubaker K 2011 *Eur. Phys. J. Plus* **126** 10
[17] Schroder D K 2006 *Semiconductor Material and Device Characterization* 3rd edn (Hoboken, NJ: Wiley) p 723
[18] Biyikli N, Aytur O, Kimukin I, Tut T and Ozbay E 2002 *Appl. Phys. Lett.* **81** 3272
[19] Bhattacharya P 1994 *Semiconductor Optoelectronic Devices* (Englewood Cliffs, NJ: Prentice-Hall)
[20] Sze M 2006 *Physics of Semiconductor Devices* 3rd edn (New York: Wiley)
[21] Look D C 2000 *Mater. Sci. Eng.* B **75** 190
[22] Bunn C W 1935 *Proc. Phys. Soc. Lond.* **47** 835
[23] Mollwo E, Breckenridge R G, Russell B R, Hahn E E (ed) 1956 *Proc. Photoconductivity Conf. (Atlantic City)* (New York: Wiley) p 509
[24] Bahnemann D W, Kormann Cl and Hoffmann M R 1987 *J. Phys. Chem.* **91** 3789
[25] Fabricius H, Skettrup T and Bisgaard P 1986 *Appl. Opt.* **25** 2764
[26] Oda S, Tokunaga H, Kitajima N, Hanna J, Shimizu I and Kokado H 1985 *Japan. J. Appl. Phys.* **24** 1607
[27] Sher A, Feleman R D, Austin R F, Opila R L, Masaitis R L, Zyskind J L and Sulhoff J W 1992 *J. Electron. Mater.* **21** 653
[28] Craciun V, Amirhaghi S, Craciun D, Elders J, Gardeniers J G E and Boyd I W 1995 *Appl. Surf. Sci.* **86** 99
[29] Ohtomo A, Kawasaki M, Koida T, Koinuma H, Sakurai Y, Yoshida Y, Sumiya M, Fuke S, Yasuda T and Segawa Y 1998 *Silicon Carbide, III-Nitrides and Related Materials* vol 264-2 (Zurich-Uetikon: Trans Tech) p 1463
[30] Vispute R D, Choopun S, Li Y H, Chalk D M, Ogale S B, Sharma R P, Venkatesan T and Iliadis A 2000 *Self-organized Processes in Semiconductor Alloys (Warrendale)* vol 583 p 189
[31] Seko A, Oba F, Kuwabara A and Tanaka I 2005 *Phys. Rev.* B **72** 024107
[32] Yang W, Hullavarad S S, Nagaraj B, Takeuchi I, Sharma R P, Venkatesan T, Vispute R D and Shen H 2003 *Appl. Phys. Lett.* **82** 3424
[33] Du X, Mei Z, Liu Z, Guo Y, Zhang T, Hou Y, Zhang Z, Xue Q and Kuznetsov A Y 2009 *Adv. Mater.* **21** 4625
[34] Liu Z L, Mei Z X, Zhang T C, Liu Y P, Guo Y, Du X L, Hallen A, Zhu J J and Kuznetsov A Y 2009 *J. Cryst. Growth* **311** 4356
[35] Liang H L, Mei Z X, Liu Z L, Guo Y, Azarov A Yu, Kuznetsov A Yu, Hallen A and Du X L 2012 *Thin Solid Films* **520** 1705–8
[36] Ohtomo A, Kawasaki M, Sakurai Y, Ohkubo I, Shiroki R, Yoshida Y, Yasuda T, Segawa Y and Koinuma H 1998 *Mater. Sci. Eng.* B **56** 263
[37] Ohtomo A, Kawasaki M, Koida T, Masubuchi K, Koinuma H, Sakurai Y, Yoshida Y, Yasuda T and Segawa Y 1998 *Appl. Phys. Lett.* **72** 2466
[38] Sharma A K, Narayan J, Muth J F, Teng C W, Jin C, Kvit A, Kolbas R M and Holland O W 1999 *Appl. Phys. Lett.* **75** 3327
[39] Park W I, Yi G C and Jang H M 2001 *Appl. Phys. Lett.* **79** 2022
[40] Takagi T, Tanaka H, Fujita S and Fujita S 2003 *Japan. J. Appl. Phys.* **42** L401
[41] Chen N B, Wu H Z, Qiu D J, Xu T N, Chen J and Shen W Z 2004 *J. Phys.: Condens. Matter* **16** 2973
[42] Tampo H, Shibata H, Maejima K, Yamada A, Matsubara K, Fons P, Niki S, Tainaka T, Chiba Y and Kanie H 2007 *Appl. Phys. Lett.* **91** 261907
[43] Choopun S, Vispute R D, Yang W, Sharma R P, Venkatesan T and Shen H 2002 *Appl. Phys. Lett.* **80** 1529
[44] Chen J, Shen W Z, Chen N B, Qiu D J and Wu H Z 2003 *J. Phys.: Condens. Matter* **15** L475
[45] Tanaka H, Fujita S and Fujita S 2005 *Appl. Phys. Lett.* **86** 192911
[46] Ryu Y R, Lee T S, Lubguban J A, Corman A B, White H W, Leem J H, Han M S, Park Y S, Youn C J and Kim W J 2006 *Appl. Phys. Lett.* **88** 052103
[47] Wang J, Dong X, Zhang B, Zhang Y, Wang H, Shi Z, Zhang S, Yin W and Du G 2013 *J. Alloys Compounds* **579** 160
[48] Su L, Zhu Y, Zhang Q, Chen M, Wu T, Gui X, Pan B, Xiang R and Tang Z 2013 *Appl. Surf. Sci.* **274** 341
[49] Yang C, Li X M, Gu Y F, Yu W D, Gao X D and Zhang Y W 2008 *Appl. Phys. Lett.* **93** 112114
[50] Yang C, Li X M, Yu W D, Gao X D, Cao X and Li Y Z 2009 *J. Phys. D: Appl. Phys.* **42** 152002
[51] Fernandez A M and Sebastian P J 1993 *J. Phys. D: Appl. Phys.* **26** 2001
[52] Sun H, Zhang Q F and Wu J L 2006 *Nanotechnology* **17** 2271
[53] Brillson L J and Lu Y 2011 *J. Appl. Phys.* **109** 123504
[54] Liang S, Sheng H, Liu Y, Huo Z, Lu Y and Shen H 2001 *J. Cryst. Growth* **225** 110
[55] Takeuchi M, Kashimura S and Ozawa S 1990 *Vacuum* **41** 1636
[56] Liu Y, Gorla C R, Liang S, Emanetoglu N, Lu Y, Shen H and Wraback M 2000 *J. Electron. Mater.* **29** 69
[57] Xu Q A, Zhang J W, Ju K R, Yang X D and Hou X 2006 *J. Cryst. Growth* **289** 44
[58] Liu K W, Ma J G, Zhang J Y, Lu Y M, Jiang D Y, Li B H, Zhao D X, Zhang Z Z, Yao B and Shen D Z 2007 *Solid-State Electron.* **51** 757
[59] Chang S P, Chang S J, Chiou Y Z, Lu C Y, Lin T K, Lin Y C, Kuo C F and Chang H M 2007 *Sensors Actuators* A **140** 60
[60] Zheng X G, Li Q Sh, Zhao J P, Chen D, Zhao B, Yang Y J and Zhang L Ch 2006 *Appl. Surf. Sci.* **253** 2264
[61] Mandalapu L J, Xiu F X, Yang Z and Liu J L 2007 *J. Appl. Phys.* **102** 023716
[62] Bi Z, Zhang J, Bian X, Wang D, Zhang X, Zhang W and Hou X 2008 *J. Electron. Mater.* **37** 760
[63] Porter H L, Cai A L, Muth J F and Narayan J 2005 *Appl. Phys. Lett.* **86** 211918

[64] Chang S P, Chuang R W, Chang S J, Lu C Y, Chiou Y Z and Hsieh S F 2009 *Thin Solid Films* **517** 5050
[65] Ji L W, Wu C Z, Lin C M, Meen T H, Lam K T, Peng S M, Young S J and Liu C H 2010 *Japan. J. Appl. Phys.* **49** 052201
[66] Hove H V and Luyckx A 1966 *Solid State Commun.* **4** 603–6
[67] Miller P H Jr 1956 *Proc. Photoconductivity Conf. (Atlantic City)* (New York: Wiley) p 287
[68] Yadav H K and Gupta V 2012 *J. Appl. Phys.* **111** 102809
[69] Moazzami K, Murphy T E, Phillips J D, Cheung MC K and Cartwright A N 2006 *Semicond. Sci. Technol.* **21** 717
[70] Murphy T E, Moazzami K and Phillips J D 2006 *J. Electron. Mater.* **35** 543
[71] Xu Z Q, Deng H, Xie J, Li Y and Zu X T 2006 *Appl. Surf. Sci.* **253** 476
[72] Sun J, Dai Q, Liu F, Huang H, Li Z, Zhang X and Wang Y 2011 *Sci. China Phys. Mech. Astron.* **54** 102
[73] Mandalapu L J, Xiu F X, Yang Z and Liu J L 2007 *Solid-State Electron.* **51** 1014
[74] Sun J, Liu F J, Huang H Q, Zhao J W, Hu Z F, Zhang X Q and Wang Y S 2010 *Appl. Surf. Sci.* **257** 921
[75] Shinde S S and Rajpure K Y 2011 *Mater. Res. Bull.* **46** 1734
[76] Rajan A, Yadav H K, Gupta V and Tomar M 2013 *J. Mater. Sci.* **48** 7994
[77] Shinde S S, Bhosale C H and Rajpure K Y 2012 *Solid-State Electron.* **68** 22
[78] Shinde S S and Rajpure K Y 2012 *J. Alloys Compounds* **522** 118
[79] Hasan K, Nur O and Willander M 2012 *Appl. Phys. Lett.* **100** 211104
[80] Shinde S S and Rajpure K Y 2011 *Appl. Surf. Sci.* **257** 9595
[81] Rajan A, Yadav H K, Gupta V and Tomar M 2013 *J. Mater. Sci.* **48** 7994
[82] Yang W, Vispute R D, Choopun S, Sharma R P, Venkatesan T and Shen H 2001 *Appl. Phys. Lett.* **78** 2787
[83] Han S *et al* 2011 *Appl. Phys. Lett.* **99** 242105
[84] Li G, Zhang K, Zhang J and Liu Y 2011 *Opt. Eng.* **50** 113801
[85] Jiang D Y, Zhang J Y, Liu K W, Zhao Y M, Cong C X, Lu Y M, Yao B, Zhang Z Z and Shen D Z 2007 *Semicond. Sci. Technol.* **22** 687
[86] Jiang D Y, Qin J M, Zhang X Y, Bai Z H and Shen D Z 2011 *Mater. Sci. Eng.* B **176** 736
[87] Wei M, Deng H, Chen H and Chen J J 2009 *Adv. Mater. Res.* **60–61** 110
[88] Zhao C Y, Wang X H, Zhang J Y, Ju Z G, Shan C X, Yao B, Zhao D X, Shen D Z and Fan X W 2011 *Thin Solid Films* **519** 1976
[89] Bethe H A 1942 *MIT Radiation Laboratory Report* No. 43-12
[90] Allen M W, Alkaisi M M and Durbin S M 2006 *Appl. Phys. Lett.* **89** 103520
[91] Sheng H, Muthukumar S, Emanetoglu N W and Lu Y 2002 *Appl. Phys. Lett.* **80** 2132
[92] Kim S H, Kim H K and Seong T Y 2005 *Appl. Phys. Lett.* **86** 112101
[93] Li Y Z, Li X M and Gao X D 2011 *J. Alloys Compounds* **509** 7193
[94] Ali G M and Chakrabarti P 2012 *J. Vac. Sci. Technol.* B **30** 031206
[95] Oh D C, Suzuki T, Hanada T, Yao T, Makino H and Ko H J 2006 *J. Vac. Sci. Technol.* B **24** 1595
[96] Peng S M, Su Y K, Ji L W, Young S J, Wu C Z, Tsai C N, Chao W C and Cheng W B 2011 *IEEE Sensors J.* **11** 1173
[97] Nakano M *et al* 2008 *Appl. Phys. Lett.* **93** 123309
[98] Dai J N, Han X Y, Wu Z H, Fang Y Y, Xiong H, Tian Y, Yu C H, He Q H and Chen C Q 2011 *J. Electron. Mater.* **40** 446
[99] Ali G M and Chakrabarti P 2010 *Appl. Phys. Lett.* **97** 031116
[100] Ali G M and Chakrabarti P 2010 *IEEE Photon. J.* **2** 784
[101] Endo H, Sugibuchi M, Takahashi K, Goto S, Sugimura S, Hane K and Kashiwaba Y 2007 *Appl. Phys. Lett.* **90** 121906
[102] Lin T K, Chang S J, Su Y K, Huang B R, Fujita M and Horikoshi Y 2005 *J. Cryst. Growth* **281** 513
[103] Young S J, Ji L W, Chang S J and Su Y K 2006 *J. Cryst. Growth* **293** 43
[104] Young S J, Ji L W, Fang T H, Chang S J, Su Y K and Du X L 2007 *Acta Mater.* **55** 329
[105] Young S J, Ji L W, Chang S J, Liang S H, Lam K T, Fang T H, Chen K J, Du X L and Xue Q K 2008 *Sensors Actuators* A **141** 225–9
[106] Liu J S, Shan C X, Li B H, Zhang Z Z, Yang C L, Shen D Z and Fan X W 2010 *Appl. Phys. Lett.* **97** 251102
[107] Li M, Anderson W, Chokshi N, Deleon R L and Tompa G 2006 *J. Appl. Phys.* **100** 053106
[108] Shan C X, Zhang J Y, Yao B, Shen D Z, Fan X W and Choy K L 2009 *J. Vac. Sci. Technol.* B **27** 1765
[109] Jiang D, Zhang J, Lu Y, Liu L, Zhao D, Zhang Z, Shen D and Fan X 2008 *Solid-State Electron.* **52** 679–68
[110] Li M, Chokshi N, Deleon R L, Tompa G, and Anderson W A 2007 *Thin Solid Films* **515** 7357
[111] Yu J, Shan C X, Huang X M, Zhang X W, Wang S P and Shen D Z 2013 *J. Phys. D: Appl. Phys.* **46** 305105
[112] Kim J, Yun J H, Jee S W, Park Y C, Ju M, Han S, Kim Y, Kim J H, Anderson W A, Lee J H and Yi J 2011 *Mater. Lett.* **65** 786
[113] Jandow N N, Yam F K, Thahab S M, Abu Hassan H and Ibrahim K 2010 *Curr. Appl. Phys.* **10** 1452
[114] Jandow N N, Ibrahim K A, Abu Hassan H, Thahab S M and Hamad O S 2010 *J. Electron Devices.* **7** 225–9
[115] Ali G M, Singh S and Chakrabarti P 2010 *J. Electron. Sci. Technol.* **8** 55–9
[116] Yu P, Li L, Lubguban J A, Ryu Y, Lee T S and White H W 2006 *AIP Conf. Proc.* **893** 1421
[117] Ji L W, Wu C Z, Lin C M, Meen T H, Lam K T, Peng S M, Young S J and Liu C H 2010 *Japan. J. Appl. Phys.* **49** 052201
[118] Lee H Y, Hsu Y T and Lee C T 2013 *Solid-State Electron.* **79** 223
[119] Nakano M *et al* 2008 *Appl. Phys. Express* **1** 121201
[120] Endo H, Sugibuchi M, Takahashi K, Goto S, Hane K and Kashiwaba Y 2008 *Phys. Status Solidi* c **5** 3119
[121] Redondo-Cubero A, Hierro A, Chauveau J M, Lorenz K, Tabares G, Franco N, Alves E and Muñoz E 2012 *CrystEngComm* **14** 1637
[122] Han S, Zhang J Y, Zhang Z Z, Wang L K, Zhao Y M, Zheng J, Cao J M, Yao B, Zhao D X and Shen D Z 2010 *J. Phys. Chem.* C **114** 21757
[123] Tabares G, Hierro A, Ulloa J M, Guzman A, Muñoz E, Nakamura A, Hayashi T and Temmyo J 2010 *Appl. Phys. Lett.* **96** 101112
[124] Zhu H, Shan C X, Wang L K, Zheng J, Zhang J Y, Yao B and Shen D Z 2010 *J. Phys. Chem.* C **114** 7169–72
[125] Xie X H, Zhang Z Z, Li B H, Wang S P, Jiang M M, Shan C X, Zhao D X, Chen H, Yao B and Shen D Z 2013 *Appl. Phys. Lett.* **102** 231122
[126] Sarver F L K J F and Hummel F A 1959 *J. Electrochem. Soc.* **106** 960
[127] Takeuchi J I, Yang W, Chang K S, Aronova M A, Venkatesan T, Vispute R D and Bendersky L A 2003 *J. Appl. Phys.* **94** 7336–40
[128] Lee H Y, Wang M Y, Chang K J and Lin W J 2008 *IEEE Photon. Technol. Lett.* **20** 2108
[129] Hou Y N, Mei Z X, Liu Z L, Zhang T C and Du X L 2011 *Appl. Phys. Lett.* **98** 103506
[130] Wang L K, Ju Z G, Shan C X, Zheng J, Shen D Z, Yao B, Zhao D X, Zhang Z Z, Li B H, and Zhang J Y 2009 *Solid State Commun.* **149** 2021

[131] Yu J, Shan C X, Liu J S, Zhang X W, Li B H and Shen D Z 2013 *Phys. Status Solidi* RRL **7** 425–8
[132] Koike K, Hama K, Nakashima I, Takada G, Ogata K, Sasa S, Inoue M and Yano M 2005 *J. Cryst. Growth* **278** 288
[133] Hou Y N, Mei Z X, Liang H L, Ye D Q, Liang S, Gu C Z and Du X L 2011 *Appl. Phys. Lett.* **98** 263501
[134] Zheng Q, Huang F, Ding K, Huang J, Chen D, Zhan Z and Lin Z 2011 *Appl. Phys. Lett.* **98** 221112
[135] Liang H L, Mei Z X, Hou Y N, Liang S, Liu Z L, Liu Y P, Li J Q and Du X L 2013 *J. Cryst. Growth* **381** 6
[136] Suhail A M, Hassan E K, Ahmed S S and Alnoori M K M 2010 *J. Electron Devices* **8** 268
[137] Hullavarad S S, Dhar S, Varughese B, Takeuchi I, Venkatesan T and Vispute R D 2005 *J. Vac. Sci. Technol.* A **23** 982
[138] Liu K W, Zhang J Y, Ma J G, Jiang D Y, Lu Y M, Yao B, Li B H, Zhao D X, Zhang Z Z and Shen D Z 2007 *J. Phys. D: Appl. Phys.* **40** 2765
[139] Jiang D, Shan C, Zhang J, Lu Y, Yao B, Zhao D, Zhang Z, Fan X and Shen D 2009 *Cryst. Growth Des.* **9** 454
[140] Zhao Y, Zhang J, Jiang D, Shan C, Zhang Z, Yao B, Zhao D and Shen D 2009 *ACS Appl. Mater. Interfaces* **1** 2428–30
[141] Zheng Q, Huang F, Huang J, Hu Q, Chen D and Ding K 2012 *IEEE Electron Device Lett.* **33** 1033
[142] Jiang D Y, Shan C X, Zhang J Y, Lu Y M, Yao B, Zhao D X, Zhang Z Z, Shen D Z and Yang C L 2009 *J. Phys. D: Appl. Phys.* **42** 025106
[143] Ju Z G, Shan C X, Jiang D Y, Zhang J Y, Yao B, Zhao D X, Shen D Z and Fan X W 2008 *Appl. Phys. Lett.* **93** 173505
[144] Han S, Zhang J, Zhang Z, Zhao Y, Wang L, Zheng J, Yao B, Zhao D and Shen D 2010 *ACS Appl. Mater. Interfaces* **2** 1918
[145] Liu W, Gu S L, Ye J D, Zhu S M, Liu S M, Zhou X, Zhang R, Shi Y, Zheng Y D, Hang Y and Zhang C L 2006 *Appl. Phys. Lett.* **88** 092101
[146] Lim J H, Kang C K, Kim K K, Park I K, Hwang D K, Park S J 2006 *Adv. Mater.* **18** 2720
[147] Look D C, Reynolds D C, Litton C W, Jones R L, Eason D B and Cantwell G 2002 *Appl. Phys. Lett.* **81** 1830
[148] Ryu Y R, Lee T S and White H W 2003 *Appl. Phys. Lett.* **83** 87
[149] Ryu Y R, Lee T S, Lubguban J A, White H W, Park Y S and Youn C J 2005 *Appl. Phys. Lett.* **87** 153504
[150] Lopatiuk-Tirpak O, Nootz G, Flitsiyan E, Chernyak L, Mandalapu L J, Yang Z, Liu J L, Gartsman K and Osinsky A 2007 *Appl. Phys. Lett.* **91** 042115
[151] Lin T S and Lee C T 2012 *Appl. Phys. Lett.* **101** 221118
[152] Moon T H, Jeong M C, Lee W, Myoung J M 2005 *Appl. Surf. Sci.* **240** 280
[153] Liu J L, Xiu F X, Mandalapu L J and Yang Z 2006 *Proc. SPIE* **6122** 61220H
[154] Mandalapu L J, Yang Z, Xiu F X, Zhao D T and Liu J L 2006 *Appl. Phys. Lett.* **88** 092103
[155] Lopatiuk-Tirpak O, Chernyak L, Mandalapu L J, Yang Z, Liu J L, Gartsman K, Feldman Y and Dashevsky Z 2006 *Appl. Phys. Lett.* **89** 142114
[156] Ohta H, Hirano M, Nakahara K, Maruta H, Tanabe T, Kamiya M, Kamiya T and Hosono H 2003 *Appl. Phys. Lett.* **83** 1029
[157] Ohta H, Kamiya M, Kamiya T, Hirano M, Hosono H 2003 *Thin Solid Films* **445** 317
[158] Wang K, Vygranenko Y and Nathan A 2007 *J. Appl. Phys.* **101** 114508
[159] Tsai S Y, Hon M H and Lu Y M 2011 *Solid-State Electron.* **63** 37
[160] Zhang X L, Hui K S and Hui K N 2013 *Mater. Res. Bull.* **48** 305
[161] Park N, Sun K, Sun Z, Jing Y and Wang D 2013 *J. Mater. Chem.* C **1** 7333–8
[162] Liu J, Xia Y, Wang L, Su Q and Shi W 2007 *Appl. Surf. Sci.* **253** 5218
[163] Huang J, Wang L J, Tang K, Zhang J J, Xia Y B and Lu X G 2012 *Appl. Surf. Sci.* **258** 2010
[164] Alivov Ya I, Özgür Ü, Doğan S, Johnstone D, Avrutin V, Onojima N, Liu C, Xie J, Fan Q and Morkoç H 2005 *Appl. Phys. Lett.* **86** 241108
[165] Oh D C, Suzuki T, Makino H, Hanada T, Ko H J and Yao T 2006 *Phys. Status Solidi* c **3** 946
[166] Zhu H, Shan C X, Yao B, Li B H, Zhang J Y, Zhao D X, Shen D Z and Fan X W 2008 *Phys. Chem.* C **112** 20546
[167] Al-Zouhbi A, Al-Din N S and Manasreh M 2012 *Opt. Rev.* **19** 235
[168] Jeong I S, Kim J H and Im S 2003 *Appl. Phys. Lett.* **83** 2946
[169] Kosyachenko L A, Lashkarev G V, Sklyarchuk V M, Ievtushenko A I, Sklyarchuk O F, Lazorenko V I and Ulyashin A 2010 *Phys. Status Solidi* a **8** 1972
[170] Park C H, Jeong I S, Kim J H and Im S 2003 *Appl. Phys. Lett.* **82** 3973
[171] Chen C P, Lin P H, Chen L Y, Ke M Y, Cheng Y W and Huang J J 2009 *Nanotechnology* **20** 245204
[172] Gupta B, Jain A and Mehra R M 2010 *J. Mater. Sci. Technol.* **26** 223
[173] Zhang T C, Guo Y, Mei Z X, Gu C Z and Du X L 2009 *Appl. Phys. Lett.* **94** 113508
[174] Tasi D S, Kang C F, Wang H H, Lin C A, Ke J J, Chu Y H and He J H 2012 *Opt. Lett.* **37** 1112
[175] Rakhshani A E 2010 *J. Appl. Phys.* **108** 094502
[176] Liu K W, Shen D Z, Shan C X, Zhang J Y, Yao B, Zhao D X, Lu Y M and Fan X W 2007 *Appl. Phys. Lett.* **91** 201106
[177] Shukla G 2009 *IEEE Photon. Technol. Lett.* **21** 887
[178] Li Y F *et al* 2009 *J. Phys. D: Appl. Phys.* **42** 105102
[179] Liu W W, Yao B, Li B H, Li Y F, Zheng J, Zhang Z Z, Shan C X, Zhang J Y, Shen D Z and Fan X W 2010 *Solid State Sci.* **12** 1567
[180] Hou Y, Mei Z, Liang H, Ye D, Gu C, Du X and Lu Y 2013 *IEEE Trans. Electr. Dev.* **60** 3474
[181] Ohotomo A, Kawasaki M, Ohkubo I, Koinuma H, Yasuda T and Segawa Y 1999 *Appl. Phys. Lett.* **75** 980
[182] Liang H L, Mei Z X, Zhang Q H, Gu L, Liang S, Hou Y N, Ye D Q, Gu C Z, Yu R C and Du X L 2011 *Appl. Phys. Lett.* **98** 221902
[183] Hou Y N, Mei Z X, Liang H L, Ye D Q, Gu C Z and Du X L 2013 *Appl. Phys. Lett.* **102** 153510
[184] Bae H S, Kim M H and Im S 2003 *Appl. Phys. Lett.* **83** 5313
[185] Bae H S and Im S 2004 *Thin Solid Films* **469–470** 75
[186] Reyes P I, Ku C J, Z Duan, Xu Y, Garfunkel E and Lu Y 2012 *Appl. Phys. Lett.* **101** 031118
[187] Lee K, Choi J M, Hwang D K, Oh M S, Kim J K, Jung Y, Oh K and Im S 2008 *Sensors Actuators* A **144** 69–73
[188] Lee K, Kim K, Choi J M, Oh M S, Hwang D K, Jang S, Kim E and Im S 2008 *J. Phys. D: Appl. Phys.* **41** 135102
[189] Chen W T and Zan H W 2012 *IEEE Electron Device Lett.* **33** 77